d/Collection

석사학위논문

CFD에 의한 반잠수식 부유식 풍력터빈의 공기역학 및 동적응답특성에 관한 연구

제주대학교 대학원

풍력공학부 풍력기계시스템 전공

장 인

2019 년 2월

CFD에 의한 반잠수식 부유식 풍력터빈의 공기역학 및 동적응답특성에 관한 연구

指導敎授 金 範 錫

張 印

이 論文을 風力工學部 碩士學位 論文으로 提出함

2018 年 12 月

張 印의 風力工學部 碩士學位 論文을 認准함

審査委員長 고경남

委　　員 김범석

委　　員 허승렬

濟州大學校 大學院

2018 年 12 月

A CFD study on aerodynamic and hydrodynamic response of semi-submersible Floating Offshore Wind Turbine

Yin Zhang

(Supervised by professor Bum-Suk Kim)

A thesis submitted in partial fulfillment of the requirement for the degree of Master of Science

2018. 12.

This thesis has been examined and approved.

Kyungnam Ko

....
Thesis director, Kyung-Nam Ko, Prof. Faculty of Wind Energy Engineering

Bum Suk, Kim

....
Thesis director, Bum-Suk Kim, Prof. Faculty of Wind Energy Engineering

....
Thesis director, Jong-Chul Huh, Prof. Mechanical Engineering

2018. 12. 05
Date

Faculty of Wind Energy Engineering

Graduate School

Jeju National University

Contents

List of figures

List of tables

Abstract

Accurate prediction of the time-dependent system dynamic responses of floating offshore wind turbine (FOWT) under aero-hydro coupled conditions is a challenge. This study modeled the NREL 5 MW wind turbine, supported by the semi-submersible platform mentioned in Phase II of Offshore Code Comparison, Collaboration, Continued, with Correlations (OC5) project, in coupled wind-wave condition via CFD method.

Finally, complex unsteady flow fields considering blade and tower interference effects among blade-tip vortices, shedding vortices, and turbulent wakes are numerically visualized and investigated in detail. Different behavior of vortices was observed when the platform motion upwind direction and downwind direction. All the 3-DOFs, including heave, surge and pitch had smaller amplitudes compared with the results in the regular wave test without wind conditions. Incoming wind from the x direction obviously has a large effect on the restoring force in the mooring line, and as a result, the whole FOWT system cannot be restored back to the equilibrium position as in the regular wave test. A relatively heavy load on the hub and blade is observed for the FOWT compared with the onshore wind turbine, a relatively heavy load on the hub and blade was observed for the FOWT compared with the onshore wind turbine, leading to a 7.8% increase in the thrust curve; a 10% decrease in the power curve was also observed for the floating type turbines, which could be attributed to the smaller project area and relative wind speed required for the rotor to receive wind power when the platform pitches. Besides, comparing with variations of thrust, power production was more sensitive to platform motion.

요약

공력-수력 연동 조건을 고려한 부유식 해상풍력터빈의 시간변화에 따른 시스템 동역학적 응답을 정확히 예측하는 것은 도전적인 문제이다. 본 연구에서는 해상 코드 비교 등을 목적으로 하는 OC5 2단계 프로젝트에 근거하여 반잠수식 플랫폼에 의해 지지되는 NREL 5MW 풍력터빈 모델을 대상으로 바람과 파도조건을 동시에 고려한 전산유체해석을 수행하였다.

블레이드와 타워의 상호작용이 고려된 팁 와류, 와 방출 및 난류 후류 등의 복잡한 비정상 유동장에 대한 수치해석 결과를 분석 및 제시하였다. 부유체 플랫폼이 바람방향 및 바람반대방향으로 거동함에 따라 서로 다른 형태의 와 방출 특성이 나타났다. Heave, surge, pitch 등의 3 자유도 운동은 바람 조건을 고려하지 않은 정규파 시험 결과에 비해 다소 작은 진폭을 갖는 것으로 확인된다. 터빈으로 유입되는 바람은 계류라인의 회복력에 큰 영향을 미치기 때문에 바람과 파도를 동시에 고려한 부유식 풍력터빈 시스템 해석 결과에서는 정규파 시험과는 달리 안정적인 위치로의 복원되지 이루어지지 않는 결과를 보인다. 육상풍력터빈에 비해 상대적으로 높은 하중이 블레이드와 허브에 작용하여 추력 곡선이 7.8% 증가하는 특징을 보였으며, 출력은 약 10% 감소하는 결과를 보였다. 즉, 부유식 풍력터빈의 경우 플랫폼의 피치 운동으로 인해 로터의 투영면적이 감소하고 블레이드 단면으로 유입되는 상대풍속이 다소 감소하는 등의 문제로 인해 출력 감소 및 하중 증대로 이어질 수 있다. 부유식 풍력터빈과 고정식 풍력터빈의 비교결과, 구조물의 거동에 의한 추력의 증가율 보다 출력의 감소율이 더 크게 나타날 수 있음을 확인하였다.

I. Introduction

1.1 Research background

Energy exhaustion and shortage is a serious security problem been faced all over the world, and energy demand of the whole world will keep growing for a long time. Wind energy has become the most promising renewable energy due to its advantages of clean and convenient utilization features.

Energy generation from offshore wind farms has been gearing the attention of researchers, owning to the abundance of resources needed and the low environmental impact. Compared with offshore wind turbines in shallow water, floating offshore wind turbine (FOWT) have more advantages[1], i.e., there are several deep-water sites suitable for installation, wind resource is more abundant in offshore areas, and public concerns on the visual and environment impacts are minimized with this technology, as shown in Fig 1-1.

Since the 1990s, the development of offshore wind turbine technology has been greatly improved. But unlike the high efficiency of offshore oil and gas production, the main problem of offshore wind turbine is the high cost, high structure makes it extremely inconvenient to install and transport. Therefore, the future development will be driven by the following trends:

- Scale of wind turbine is getting larger, wind farm will gradually developing from single unit or small wind farm into large and medium-sized wind farm.
- The layout and control of wind farms are further optimized, and the technical cost is gradually reduced.
- From the shallow sea to the deep sea, offshore wind turbine has gradually developed from a fixed support structure to a floating support structure. The research and test technology of offshore floating structure will become a hot spot.
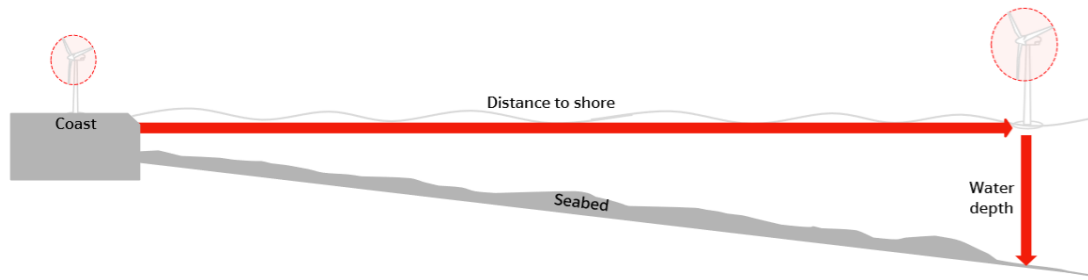
Fig 1-1. Offshore wind turbine development trend

As early as the 1970s, Europe began the demonstration of offshore wind farms, and it wasn't until the 1990s that the prototype was completed. In 1990, Sweden installed the world's first offshore wind turbine. Since then, Britain, Denmark and the Netherlands have built and successfully operated several offshore wind farms. China has also invested much in offshore wind farms in recent years, many offshore wind farms has been built, such as the bohai offshore wind farm and the donghai bridge offshore wind farm as shown in Fig 1-2. Donghai bridge offshore wind farm is the Asia's first offshore wind power project. The project was officially put into operation in July 2010, with 34 wind turbines installed, each with a capacity of 3MW and a total installed capacity of 102MW. But at present, the study of floating offshore wind turbine is still in theoretical analysis and experimental research stage. Some floating wind farms have been installed, e.g., the 1st full- scale 2.3- MW FOWT was installed in Hywind near the coast of Norway, and last year, five 6- MW FOWTs were installed in North Sea off the coast of Peterhead, Scotland.

(**a**)   (**b**)

(**c**)

Fig 1-2. Offshore wind farm; (**a**) Donghai bridge offshore wind farm (**b**) 1st full-scale 2.3MW Hywind floating

offshore wind turbine (**c**) 1st commercial FOWT wind farm

1.1.1 *Offshore wind turbine foundation structures*

As most of the established offshore wind farms are located in shallow offshore waters, the support structure forms are almost fixed foundation, most of which is monopole type. Besides, offshore support structure include gravity type, jacket type and tripod type. As shown in Fig 1-3
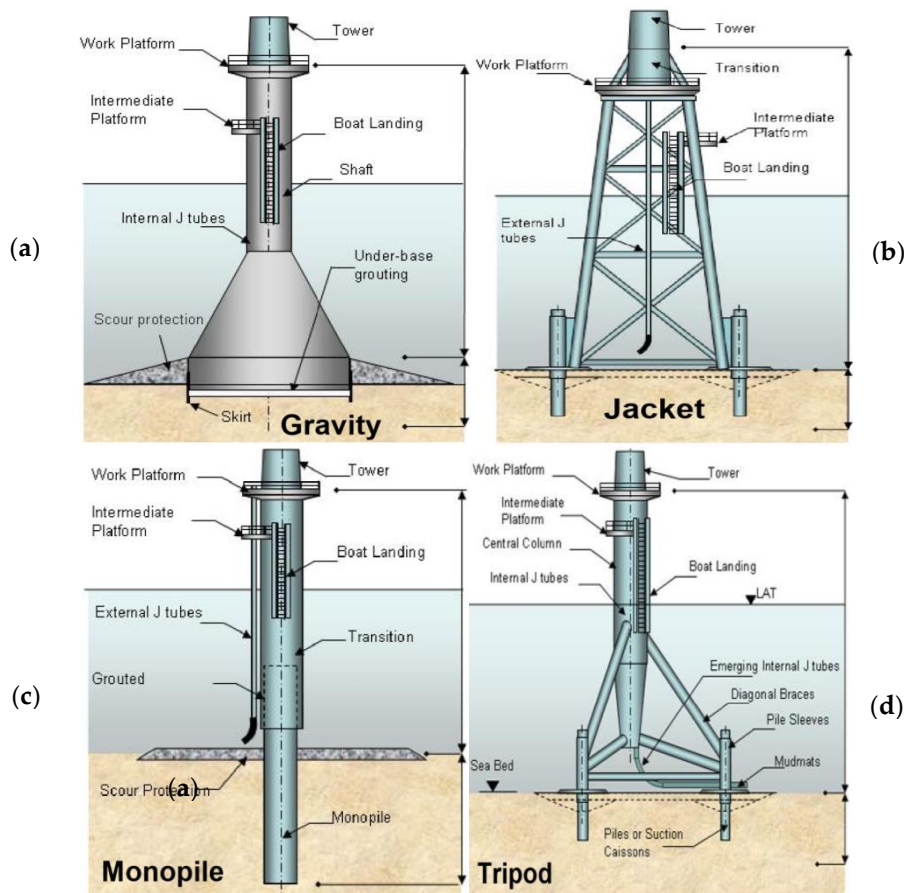
Fig 1-3. Fix type foundation structure; (**a**) Gravity type; (**b**) Jacket type; (**c**) Monopile type; (**d**) Tripod type

With the increase of the water depth, the wind turbine scale is gradually becoming larger, fixed type construction can no more support capacity over 5MW. As a result, the foundation structure of offshore wind turbine developing from fixed type to floating type. Since the 1990s, scholars of various countries have carried out researches on offshore floating wind turbines and put forward various conceptions. As shown in Fig 1-4. Most of these models refer to the structure of offshore platforms, mainly including spar type, TLP type, and semi-submersible type. Features of 3 floating type have been surmised as Table 1-1.

Fig 1-4. The floating foundation of offshore wind turbine

Spar type:

Similar to the offshore oil field, the foundation structure of spar type is a cylindrical structure, which is filled with rocks and other objects for ballasting and counterweight, and is fixed by a mooring line system on the platform. By adjusting ballast at the bottom of platform, to keep the center of gravity lower than buoyancy center, so as to provide recovery torque and ensure the stability of the platform. The spar type platform maintains the position of wind turbine though the mooring lines. Compared with other mooring systems, the cost of spar structure will be reduced by nearly half.

Semi-submersible：

Semi-submersible type is mainly composed of platform body, vertical column and floating box in bottom part. There are also some diagonal supports between platform and vertical columns, main platform body is above water surface to reduce wave impact, and the buoyancy force is provided by floating box, which below the water surface to reduce wave impact. The stability of the structure depends on the balance of gravity and buoyancy. Draft of semi-submersible type is small and has good stability. Compared with the other two types, the semi-submersible type is cheaper and has larger deck space, the installation and transportation of semi-submersible type is also convenient than spar and TLP types.

Tension Leg Platform (TLP) Type

TLP type is a compliant structure, which generally includes platform body, tension leg system and anchorage system. Through its specific structure, it generates buoyancy far beyond self-weight, and the remaining buoyancy is provided to the tension leg system to make it in the restressed state, reduce platform movement. The anchorage foundation part not only bears various loads of platform and seabed, but also provides sufficient stability for the structure.

Table 1-1. Comparison between different types floating platforms

Floating types	Advantage	Disadvantage
Spar type	Deep draft	Large response in roll and
	Relatively small water contact	pitch
	surface	
	Good response in heave	
	Low mooring system cost	
Semi-submersible type	Small draft	No obvious disadvantage
	Good stability	
	Large deck space	
	Install/transport easy	

TLP type	Good response in heave and roll	High cost of mooring system installation

Challenges in FOWT design process

Compared with offshore floating oil industry, the design of FOWT has just started and still faces many problems. Through the research works of many researchers, those problems are as follows:

- *Higher requirements for wind turbines*

Compared with fixed type wind turbine, the FOWT moves more violently in the marine environment. FOWT's tower is generally higher, some even up to 100 meters, so even platform in a slight movement, in the tower top may suffer violent movement. When the tower oscillates back and forth, working environment is the relative speed between the tower and incoming wind. FOWT has higher requirements to designer, such as blade design strength, which can adapt to the control strategy of offshore wind power generation.

- *Design guideline of FOWT*

The design of FOWT needs to consider not only the wave load, current load and interaction between parts, but also load on wind turbine, which an important load in the design stage. At present, there is no specific rule in designing FOWT, although the FOWT design is mentioned in Norske Veritas, Germany Lloyd's register and American bureau of shipping, but it is not specified in detail.

- *Lack of numerical simulation tools*

Due to the characteristics of the FOWT system itself, the numerical tools of simulating load and movement in fixed type wind turbine and offshore oil industry cannot be directly applied in FOWT system.

- *The reliability of model test needs further verification*

Ocean engineering structures in a given movement condition of marine environment, researcher mainly adopts numerical computation and physical model test method, during calculation, many assumptions and empirical data has introduced,

however, can lead to poor results. Engineering general calculation result will be used for preliminary design, and physical model experiment results usually used in final design. The problem of physical test model of FOWT is more prominent. Compared with the fixed type wind turbine, it is more difficult to apply load on blades in FOWT, moreover, it is impossible to use scale-down model which satisfy several laws or simulate in the wind tunnel. If the turbine is simplified, the load cannot be consistent with actual load, Therefore, the model test technology needs further research and development.

- *Cost control*

The biggest difference between FOWT and offshore oil exploitation lies in the scale of their operations. The number of offshore wind turbines must be large enough to generate economic benefits from the formation of offshore wind farms. Therefore, the design of FOWT must take into account the optimization cost and reduce the difficulty of construction and installation. For mooring system, the motion response should be guaranteed and low cost should be considered. Therefore, further optimization of the control of wind farms, and make efforts to improve the economy of FOWT can effectively ensure the rapid development of the wind power industry.

Floating offshore wind farm projects

At present, many countries and companies in Europe have shown great interest in floating offshore wind power, the install capacity is also increasing. At the same time, the floating platform type is not only limited to Spar, TLP and semi-submersible, more new types, combine their advantages, are in the research and development stage. As Table 1-2 shown.

Table 1-2. Floating offshore wind farm projects

Project	Project capacity	Country	Turbine model	Time	Type
Hywind Scotland	30MW	England	5×SWT-6.0-154	2017	Spar
Windfloat Atlantic	25MW	Portugal	3×V164-8.0	2019	Semi-submersible
Flocan 5 Canary	25MW	Spain	5×5MW	2020	Semi-spar

Nautilus Demonstration	5MW	Spain	1×5MW	2020	Semi-submersible
SeaTwirl S2	1MW	Sweden	1×1MW	2020	Spar
Kincardine	50MW	England	1×V80-2MW 6×8.4MW	2020	Semi-sub/Semi-spar
Forthwind Project	12MW	England	7×2B Energy turbine	2020	SATH SPM platform
EFGL	24MW	France	4×Haliade 150-6MW	2021	Semi-submersible
Groix-Belle-lle	24MW	France	4×Haliade 150-6MW	2021	Semi-submersible
PGL Wind Farm	24MW	France	3×SWT-8.0-154	2021	TLP
EolMed	25MW	France	4×Senvion 6.2M152	2021	Semi-submersible
Hywind Tampen	88MW	Norway	11×SWT-8.0-154	2022	Spar
Total	**333MW**				

1.2 Investigations in previous study

However, it is difficult and expensive to operate a real-scale test model and accurately calculate critical loads because the complex multi-physical phenomena are not easy to simulate in reality. In addition, this technology is dependent on extreme weather situations (such as 25 m/s cut-out speeds). Thus, the use of computational methods, involving virtual full-scale modeling, may increase the development of the controllers' reliability (such as structure and loads) of FOWTs, reduce the risks involved, and build confidence in the design stage. Among the codes used, one of the most famous ones is the FAST code, which was developed by the National Renewable Engineering Lab (NREL) based on the blade element momentum (BEM) theory[2]. However, the BEM theory is seldom applied in FOWT

situations owing to its theoretical limitation. In contrast, the fluid structure interaction (FSI) simulations, as a modern computational analysis method, has proven to be an accurate and convincing method for considering aero-hydro-servo-elastic problems; however, complex fluid conditions and blade deformation presents significant computational challenges.

Further, correctly simulating the movement of floaters on free surfaces is also a major challenge; many researchers from different institutions have developed various codes and solvers to simulate the hydrodynamic performance of floaters. Nearly all solvers are based on the following theories: the potential-based panel approach and Morrison equation. The former cannot determine viscous flow details and is usually used together with the damping coefficient obtained from experimental test data. The FAST code HydroDyn module has applied this method. The Morison equation is a semi-empirical equation; this equation mainly describes the inline force in oscillatory flow conditions; this also has theoretical limitations and it cannot adequately describe the time-dependent force. Examples include WAMIT, TimeFloat, and CHARM3D. However, there are still some physical phenomena that cannot be fully described. While the unsteady computational fluid dynamics (CFD) approach can simulate considering all physical effects, including flow viscosity, hydrostatic forces, wave diffraction, radiation, wave run-up, and slamming, and provide reliable and accurate results regarding the platform movement.

Owing to the reasons mentioned above, the CFD method is widely considered an effective and reliable method to simulate the FOWT problem; till date, several CFD-related investigations have been performed. However, previous studies have used the following methods, ignoring some effects, leading to inaccurate results. First, to investigate the hydrodynamic load and motion response of a platform on an FOWT, some studies just simplified the problem into wind turbine aerodynamic loading or ignored the tower and rotor-nacelle-assembly. Second, some studies focused on aerodynamic loading but restricted the motion of the floating platforms to a prescribed position or did not allow the platform to move with 6 DOFs.

Unai Fernandez-Gamiz et al.[3] developed an improved BEM-based solver to verify the NREL 5-MW wind turbine and determined the bending moment and thrust force in the

blade root; they also investigated rectangular sub-boundary layer vortex generators using the CFD method[4], which showed the highest vortex generator suitable for separation control. Nematbakhsh et al. [5] developed a CFD spar model and successfully captured strong nonlinear effects, which cannot be captured using the FAST code. Furthermore, their study also observed that when the wave amplitude was large, a discrepancy could exist between CFD and FAST. Vaal et al. [6] used the BEM method to investigate the surge motion of FOWTs. This showed that the BEM method could only provide a reasonable solution under slow surge motion condition; this is because in this condition, the wake dynamics could be ignored. Zhao and Wan [7] used a naoe-FOAM-SJTU simulated OC4 platform to study the effects of the presence of wind turbines. They carried out platform pitch motions at high wind speeds and investigated the wind turbine effect on the floating platform. Tran et al. [8] set the platform to execute a prescribed sinusoidal pitching motion and changed the motion amplitudes and frequencies, instead of modeling a floating platform with 6 DOFs using the unsteady BEM theory, generalized dynamic wake (GDW), and CFD; large discrepancies were observed when the pitch amplitude increased to 4°. Tran et al. [9] analyzed an FOWT system under a prescribed sinusoidal surge motion, and found that thrust and power varied significantly, which is related to the oscillation frequency; the surge motion amplitude also varied significantly. Liu et. [10] superimposed 3 DOF platform motions (surge, heave, and pitch) and concluded that the platform motion significantly impacted the thrust and torque of the wind turbine. Ren et al. [11] used FLUENT analysis for a 5-MW tension-leg-platform-type turbine under coupled wave-wind conditions and validated the simulation results against experimental data. They only considered the surge motion and concluded that during the variation in the average/mean surge response of the system, aerodynamic forces played the main role. Quallen et al. [12] performed a CFD simulation involving an OC3 spar-type FOWT model under wind-wave excitation conditions. The mean surge motion predicted using the CFD model was 25% less than that predicted using FAST. Tran and Kim [13] modeled an OC4 semi-submersible FOWT using the dynamic fluid body interaction (DFBI) method and an overset mesh technique under wind-wave excitation conditions. A good overall agreement was found between the CFD

results and FAST data. Both codes used the quasistatic method for modeling the mooring lines. S. Gueydon et al. [14] modeled a semi-submersible platform using the aNyPHATAS code to investigate operating rotor effects on drift motions and additional damping. Chen et al. [15] modeled a semi-submersible FOWT with two different blade configurations in a wave basin to further optimize the blade design for FOWTs. A. J. Dunbar et al. [16] developed an open-source CFD/6-DOF solver based on OpenFOAM and compared rotational and translational motions with FAST, demonstrating the accuracy of this tightly coupled solver.

1.3 Research objectives

The main purpose of this study was to conduct a virtual test of a real-scale 5-WM semi-submersible FOWT using the advanced CFD method. The hydrodynamic responses were validated using the latest physical test data of the Offshore Code Comparison, Collaboration, Continued, with Correlations (OC5) projects. Full- configuration FOWT simulations, simultaneously considering the rotating blade motion with 6-DOF platform dynamics were performed; a relatively large discrepancy in the predicted power was observed owing to the different properties of the mooring line and rotating inertia moment between the OC4 and OC5 projects. This proves high infinity result of OC5 project. Further, this study may provide some reference for the validation of the CFD method for use in the OC5 Phase II system and high-fidelity simulation investigations of FOWTs in coupled aero-hydro conditions.

The OC5 DeepCWind semi-submersible floating wind turbine model was used for the investigation, which is briefly described in Section 2. The numerical methods used in the study are introduced in Section 3. The aerodynamic validation studies performed using different modeling tools are briefly presented in Section 4. Section 5 presents the results of the dynamic responses of the floating system under regular wave conditions. Section 6 presents the simulation results of the fully-coupled configuration. Section 7 presents the conclusions of the study.

II. Floating offshore wind turbine model

2.1 Model description

In February of 2009, Jonkman et al. of the national renewable energy laboratory (NREL) developed a representative and practical wind turbine, which called NREL offshore 5-MW baseline wind turbine. The wind turbine is a three blade, up-wind turbine, which adopts pitch control of variable speed. A semi-submersible FOWT tested in Phase II of the OC5 project was investigated. The design parameters of the full-scale OC5 DeepCWind semi-submersible platform are summarized in Table 2-1.

Table 2-1. Full system structural properties

Parameters	Value
Mass	1.3958E+7 kg
Draft	20 m
Displacement	1.3917E+4m3
CM location below SWL	8.07 m
Roll inertia about system CM	1.3947E+10 kg-m2
Pitch inertia about system CM	1.5552E+10 kg-m2
Yaw inertia about system CM	1.3692E+10 kg-m2

The NREL 5-MW baseline wind turbine model was set above the tower, 87.6 m from water surface; we used airfoil data from the DOWEC project, which is also mentioned in Jonkman's work [1] from NREL. The major properties of the NREL 5-MW baseline wind turbine are given in Table 2-2;

Table 2-2. Blade structural properties

Parameters	Value
Length(w.r.t.root along axis)	61.5 m
Overall(integrated) mass	2.2333E+4 kg

Second mass moment of inertia	1.48248E+7 kg-m2
First mass moment of inertia	4.5727E+5 kg-m
CM location	20.475 m

The cross-sections of the rotor blade were composed of a series of DU and NACA 64 airfoils from the hub to the tip of the out-board section. The CAD model of the blade was first developed using Solidworks software, as shown in Fig 2-1.
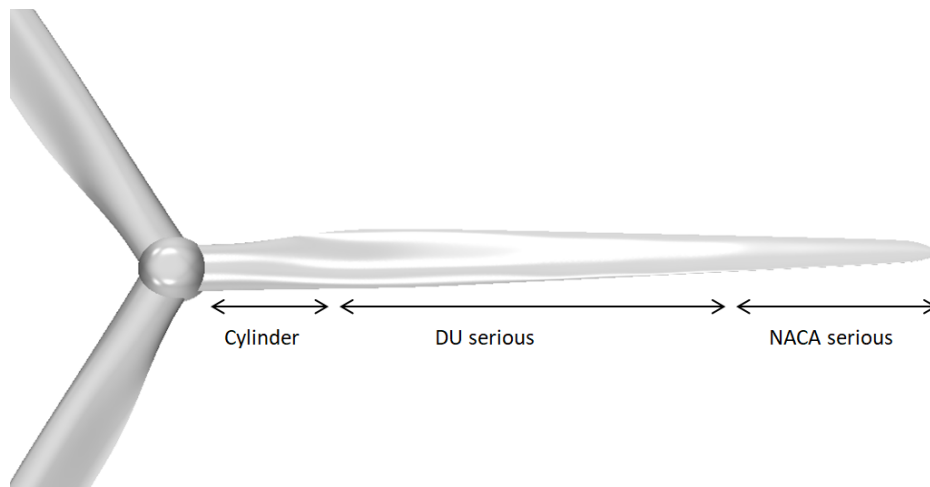

Fig 2-1. Airfoil construction of NREL 5MW blade

Except for the cylinder in the blade root and transition section, the control airfoil spread alone the blade includes the DU series airfoil from 40% to 21% thickness and an NACA airfoil of 18% thickness. Details concerning the wind blade aerodynamics including the blade twist, chord length, and airfoil designation, are presented in Table 2-3.

The 5MW semi-submersible FOWT is designed to be installed in deep sea condition with a depth of 200m, the environmental parameters of the target area are shown in the Table 2-4. Among them, the cut-in speed represents the working condition when the wind turbine begins to produce power. At this time, the wind turbine is just starting and the load is very small, which can be almost ignored. The rated working condition is the most important working condition of the wind turbine, because the wind turbine reaches the rated power production under the rated wind speed.

Table 2-3. Blade airfoil distribution of NREL 5MW wind turbine

Node radius(m)	Twist angle(deg)	Chord length (m)	Airfoil designation
2.867	13.308	3.542	Cylinder
5.600	13.308	3.854	Cylinder
8.333	13.308	4.167	Cylinder
11.750	13.308	4.557	DU 40
15.850	11.480	4.652	DU 35
19.950	10.162	4.458	DU 35
24.050	9.011	4.249	DU 30
28.150	7.795	4.007	DU 25
32.250	6.544	3.748	DU 25
36.350	5.361	3.502	DU 21
40.450	4.188	3.256	DU 21
44.550	3.125	3.010	NACA 64-618
48.650	2.319	2.764	NACA 64-618
52.750	1.526	2.518	NACA 64-618
56.167	0.863	2.313	NACA 64-618
58.900	0.370	2.086	NACA 64-618
61.633	0.106	1.419	NACA 64-618

Wind turbine is in the normal power generation state, which can achieve the maximum power generation efficiency. The maximum working condition is when the wind reaches the cut-out wind speed. At this time, the wind turbine is at the critical point between running and stopping. Once the wind speed is greater than the cut-out speed, the wind turbine stops running immediately to enter into shout down state. The extreme operating condition represents the survival condition of the wind turbine in a storm. At this time, the wind speed and wave reach the extreme value once in 50 years. The offshore wind turbine, just as platform of deep sea oil industry, has stopped working. Thus in the design and analysis stage of FOWT, the safety of wind turbine, platform and mooring line system should be ensured at this time.

Table 2-4. Working condition of DeepCWind FOWT

Wind conditions	Wind speed (m/s)	Wind direction
Cut-in speed	3	Wave advancing direction
Rated speed	11.4	Wave advancing direction
Cut-out speed	25	Wave advancing direction
Survive speed	50	Wave advancing direction

The floating platform for this model is a semi-submersible. It is considered to be buoyancy stabilized because rotational displacements induce large buoyant-restoring forces from the volumes of water that are displaced. Dimensioned drawings of the DeepCwind semi-submersible platform are given in Fig 2-2 along with the coordinate system employed in this study. The platform is made up of three offset columns with larger diameter lower bases, one center support column for the turbine, and a series of horizontal and diagonal cross bracing. The 1.6-m-diameter cross bracing consists of two sets of three pontoons connecting the outer columns with each other, two sets of three pontoons connecting the outer columns to the center column, and three diagonal braces connecting the top of the outer column to the bottom of the center column. Concerning platform flexibility, the 1/50th-scale platform was designed to be very stiff and was assumed to be rigid for the analyses conducted in this work.
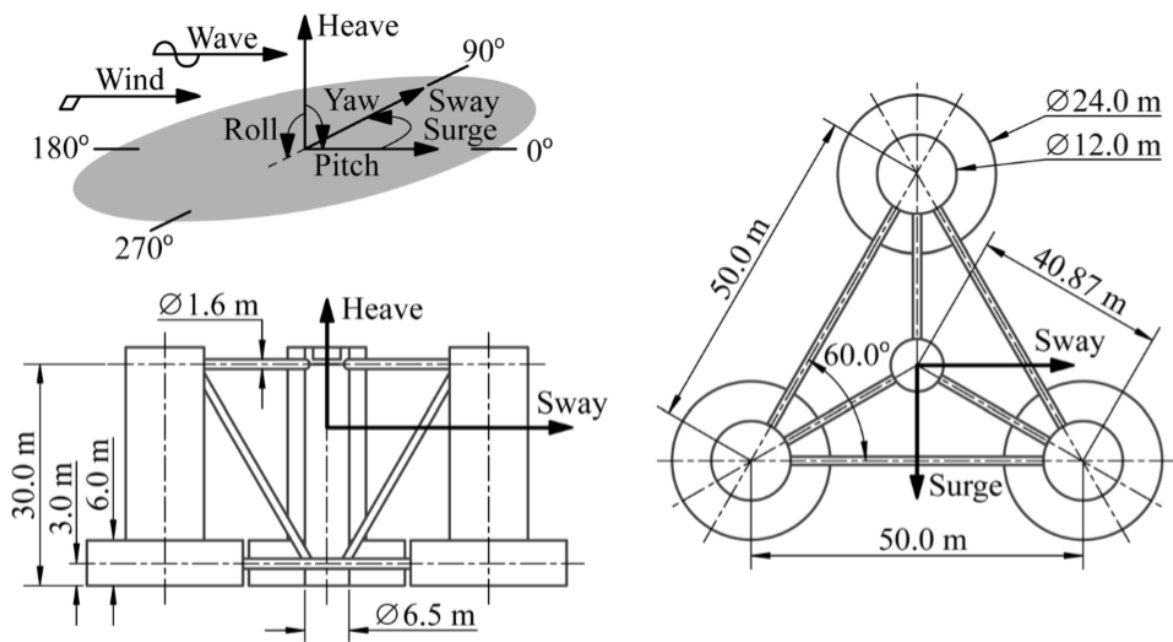

Fig 2-2. Geometry data of semi-submersible platform

2.2 OC4 and OC5 projects

Previous studies mostly used test data from the study down by Coulling et al. [12], which was led by the University of Maine at the MARIN offshore wave basin in 2011, however, the geometrically scaled model did not perform as expected under the low-Reynolds number wind conditions. In addition, only semi-submersible properties (center of mass, inertia force, etc) were considered in the OC4 project, while the OC5 project considered the properties of the full system, and the mooring line properties could be adjusted. Hence, a new scale model was built that resulted in better scaled thrust and torque loads. However, this turbine was retested in 2013, and this reset is what was examined in Phase II of the OC5 project [13]. The different physical properties of the semi-submersible platforms between the two projects are summarized in Table 2-5. Till now, most CFD studies are based on scale-model from OC4 project, while our study focus on the latest data obtained from OC5 Phase II project, as shown in Fig 2-3.

Table 2-5. Comparison of OC4&OC5 project

Semisubmersible platform	OC5 Phase II	OC4 Phase II
Mass	12919000 kg	13444000 kg
Draft	20 m	20 m
CM below SWL	14.09 m	14.4 m
Roll inertia	7.5534 E9 kg/m^2	8.011 E9 kg/m^2
Pitch inertia	8.2236 E9 kg/m^2	8.011 E9 kg/m^2
Yaw inertia	1.3612 E10 kg/m^2	1.391 E10 kg/m^2
Buoyancy center below SWL	13.15 m	
Mooringline anchors from center	837.6 m	837.6 m
Mooringline fairlead from center	40.868 m	40.868 m
Unstretched mooringline length	835.5 m	835.5 m
Mooringline mass density	Line 1: 125.6 kg/m Line 2: 125.8 kg/m Line 3: 125.4 kg/m	113.35 kg/m
Mooringline extensional stiffness	Line 1: 7.520 E8 N Line 2: 7.461 E8 N Line 3: 7.478 E8 N	7.536 E8 N
6 DOF Natural Periods	Surge: 107 s	Surge: 107 s

Sway: 112 s	Sway: 113 s
Heave: 17.5 s	Heave: 17.5 s
Roll: 32.8 s	Roll: 26.9 s
Pitch: 32.5 s	Pitch: 26.8 s
Yaw: 80.8 s	Yaw: 82.3 s

The turbine is a 1/50th scale horizontal-axis model of the NREL 5-MW reference wind turbine with a flexible tower affixed atop a semi-submersible platform. The DeepCwind semisubmersible platform is composed of a main column and three offset columns linked to the main column via several pontoons and braces; as mentioned in the OC5 report [18], the 1/50th scale and full scale models are shown in Figure 2-4. A 5-MW baseline wind turbine is vertically mounted on the main column so that the hub height from the sea surface is 90 m. In addition, the platform is moored with three catenary mooring lines, with fairleads located at the base columns. The anchors are located 200 m below the sea surface, on the seabed. One mooring line is aligned in the wave direction, which is also the platform surge direction; the others two mooring lines are distributed around the platform uniformly, and the attachment angle between each mooring line is 120°.
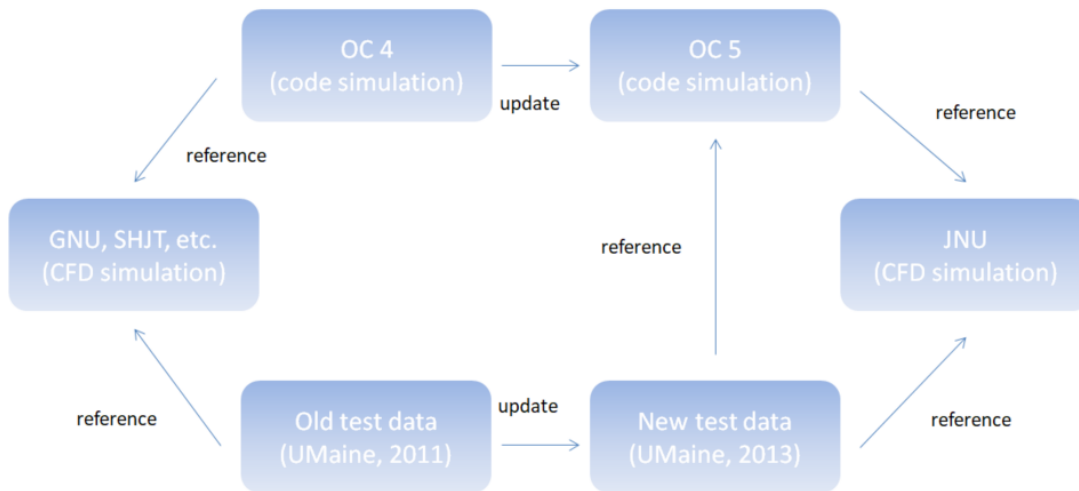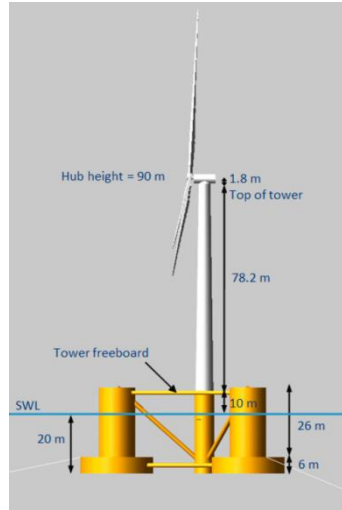

Fig 2-3. Papal study flowchart

Fig 2-4. Semi-submersible model: (**a**) Full scale model; (**b**) The 1/50th scale model in MARIN wave basin

III. Simulation Method

3.1 Numerical setting and governing equations

This paper presents a numerical modeling tool using commercial CFD software, STAR-CCM+(V12.02.010), to perform a fully coupled dynamic analysis of the DeepCwind semi-submersible floating platform with the NREL 5-MW baseline wind turbine model under combined wind-wave excitation conditions.

This investigation used the unsteady incompressible Navier-Stokes equations, according to the first principles of the conservation of mass and momentum. To solve the pressure-velocity coupling, a semi-implicit method was used, which involved a predictor-corrector approach. Second-order upwind and central difference schemes were used for the convection terms and temporal time discretization, respectively. The control equation, based on the three-dimensional viscous incompress time-average Navier-Stokes equation. The continuity and momentum equation are:

$$\frac{\partial \overline{u}_i}{\partial x_i} = 0 \tag{3.1}$$

$$\frac{\partial \overline{u}_i}{\partial t} + \overline{u}_j \frac{\partial \overline{u}_i}{\partial x_j} = -\frac{1}{\rho}\frac{\partial \overline{p}}{\partial x_i} + v\frac{\partial^2 \overline{u}_i}{\partial x_i \partial x_j} - \frac{\partial \overline{u_i' u_j'}}{\partial x_j} \tag{3.2}$$

Here, x_i is coordinate components for i direction, $\overline{u}_i$ is time domain term of velocity for i direction, u_i' is the transient term of velocity for j direction.

Additionally, the shear stress transport (SST) k-ω turbulence model (Menter's Shear Stress Transport) is a robust two-equation eddy-viscosity turbulence model used for many aerodynamic applications to resolve turbulent behavior in the fluid domain, which was first introduced in 1995 by F.R. Menter [19]. The model combines the k-ω and k-e turbulence models; therefore, the k-ω turbulence model can be used in the inner region of the boundary, and the to k-e turbulence model can be used in free shear flow. Menter's SST turbulence

model can be expressed as follows:

$$\frac{\partial(\rho k)}{\partial t} + \frac{\partial(\rho u_i k)}{\partial x_i} = \frac{\partial}{\partial x_j}\left(\Gamma_k \frac{\partial k}{\partial x_j}\right) + \overline{G}_k - Y_k + S_k \tag{3.3}$$

$$\frac{\partial(\rho \omega)}{\partial t} + \frac{\partial(\rho u_i \omega)}{\partial x_i} = \frac{\partial}{\partial x_j}\left(\Gamma_\omega \frac{\partial \omega}{\partial x_j}\right) + G_\omega - Y_\omega + D_\omega + S_\omega \tag{3.4}$$

Here, $\overline{G}_k$ represents the turbulent kinetic energy generated by the average velocity gradient, G_ω represents the turbulence dissipation rate, Γ_k and Γ_ω indicates the effective diffusivity terms of k and w due to turbulence respectively, D_ω represents the lateral dissipation derivative term, S_k and S_ω represent user-defined source items.

To obtain details of the free surface between air and water, the unsteady CFD method with the volume of fraction (VOF) approach coupled with the 6 DOF solver was used for the hydrodynamic analysis considering the surge, sway, heave, roll, pitch, and yaw motions of the platform.

3.2 Dynamic fluid body interaction（DFBI）method

The dynamic fluid body interaction (DFBI) module was applied to simulate the motion of the rigid FOWT body in response to pressure and shear forces in the fluid domain and to consider the recovery force from the mooring lines. STAR-CCM+ was used to calculate the resultant force and moment acting on the body due to various influences and also to solve the governing equations of rigid body motion to determine the new position of the rigid body. A flow chart illustrating DFBI method is shown in Fig 3-1.
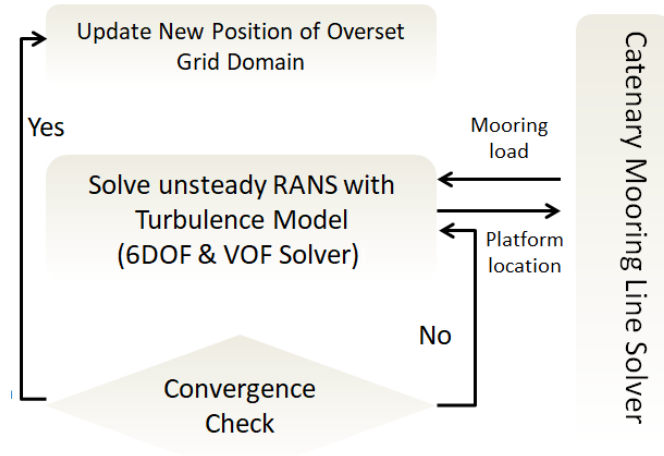
Fig 3-1. Flowchart of DFBI method

A rigid body can be defined as an object in which the relative distance between internal points does not change. Using the standard Cartesian coordinate system as a reference frame, it is possible for a rigid body to move along each of the three axes, and to rotate about the axes. As Fig 3-2 shown.
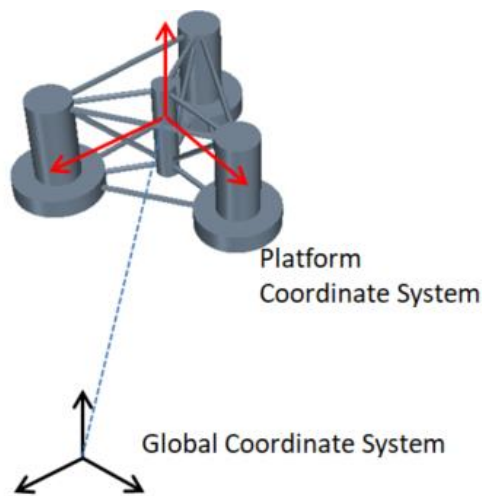

Fig 3-2. Cartesian coordinate system

For rigid bodies, it is sufficient to model the motion of the center of mass of the body alone. The relative motion of any other part of the body can be extrapolated from this center of mass. It is necessary to know the moments of inertia of the body about a fixed reference

point (which is normally the center of mass) before the rotational motion can be known. The equation for the translation of the center of mass of the body is noted in the global inertial coordinate system:

$$m\frac{dv}{dt} = f \tag{3.5}$$

Where m represents the mass of the body, f is the resultant force acting on the body and v is the velocity of the center of mass. The equation of rotation of the body is formulated in the body local coordinate system with the origin in the center of mass of the body:

$$M\frac{d\vec{\omega}}{dt} + \vec{\omega} \times M\vec{\omega} = n \tag{3.6}$$

Where M is the tensor of the moments of inertia, $\vec{\omega}$ is the angular velocity of the rigid body and n is the resultant moment acting on the body. The tensor of the moments of inertia is expanded as:

$$M = \begin{pmatrix} M_{xx} & M_{xy} & M_{xz} \\ M_{xy} & M_{yy} & M_{yz} \\ M_{xz} & M_{yz} & M_{zz} \end{pmatrix} \tag{3.7}$$

As this tensor is a symmetric, it can be defined by two vectors: one specifying the principal components along the diagonal, and another specifying the off-diagonal components.

3.3 Overset mesh technology

The overset mesh technique, also called overlapping or chimera grids, was applied. A new internal interface node was created within overset mesh region. This volume-type interface enables coupling of solutions on the domains using automatically generated sets of

- 24 -

acceptor cells in one mesh and donor cells in another mesh. Varying values of the donor cells affect the values of the acceptor cells based on interpolation. This method can handle complex geometry and body motion in dynamic simulations. The general workflow for using an overset mesh involves the steps that are outlined below.
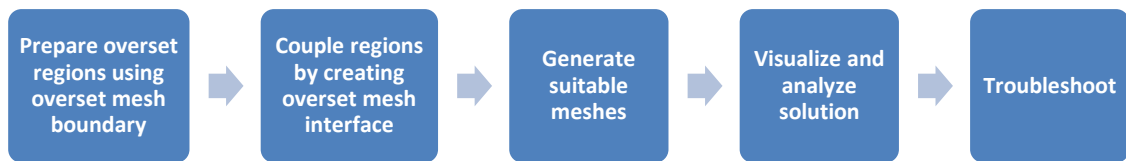

Fig 3-3. Overset mesh flowchart

To establish the connectivity between the background and the overset regions, a two-step overset assembly process takes place: First step is hole-cutting, which determines which cells are active, inactive, or acceptor cells. Second step is donor search, which ensures that donor cells are found for each acceptor cell.

The hole-cutting process is part of the coupling of the overset region with the background region through an overset interface. A successful coupling by use of an overset interface results in a "hole" being cut in the background mesh- the hole-cutting process. The hole-cutting process determines whether cells are active of inactive in the coupled simulation.

For each acceptor cell, donor cells must be found. The set of donor cells depends on the interpolation option that is chosen and on the number of active cells in the donor region around the acceptor cell centroid. The fluxes through the cell face between the last active cell and the acceptor cell are approximated in the same way as between two active cells. However, whenever the variable value at the acceptor cell centroid is referenced, the weighted variable values at the donor cells are substituted:

- 25 -

$$\emptyset_{acceptor} = \sum \alpha_i \emptyset_i \qquad (3.8)$$

In this equation, α_i is the interpolation weighting factor, $\emptyset_i$ is the value of the dependent variable $\emptyset$ at donor cells and subscript i runs over all donor nodes of an interpolation element, donor cells are represented by the green triangles in the Fig 3-4.
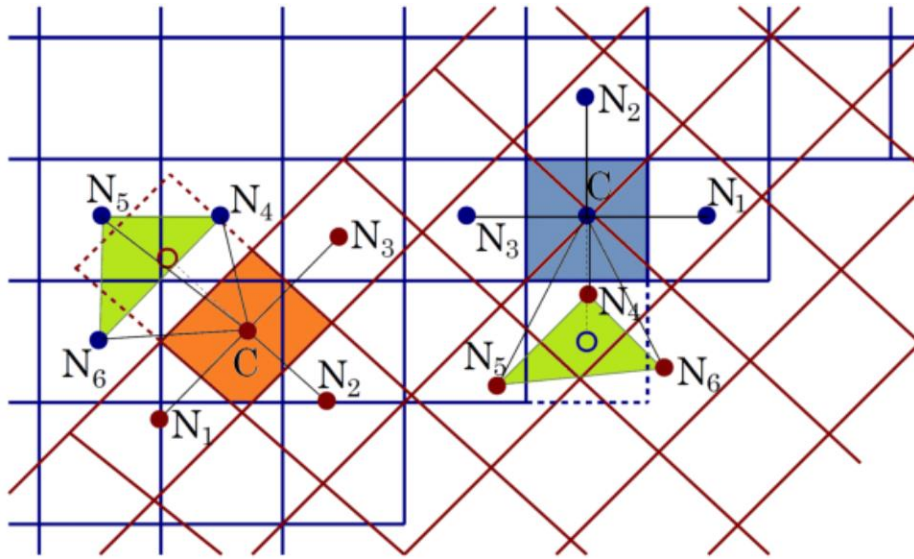

Fig 3-4. Overset mesh theory

3.4 Mooring line modeling and damping

The catenary coupling model is used to model an elastic, quasi-stationary catenary (such as a chain or towing rope), that hangs between two end points, being subject to its own weight in the field of gravity. In a local Cartesian coordinate system, the shape of the catenary is given by the following set of parametric equations:

$$x = au + bsin(u) + \alpha \qquad (3.9)$$

$$y = \mathrm{acosh}(u) + \frac{b}{2}sinh^2(u) + \beta \qquad (3.10)$$

$$for\ u_1 \leq u \leq u_2 \qquad (3.11)$$

제주대학교 중앙도서관
JEJU NATIONAL UNIVERSITY LIBRARY

Examples of where this element could be used are in modeling a tugboat and its payload, or a moored vessel and its associated tether. Quasi-stationary means that the catenary has its steady state shape at each instant of time. This model is appropriate for body motions which are sufficiently slow compared to the wave velocity in the catenary. For a coupling between a body and the environment, the system becomes as follows, f1 and f2 are tangential to the catenary curve.

There is a known limitation of the catenary coupling method: the end points of the coupling must not become vertically aligned, as this result in a singularity in the underlying catenary equation.
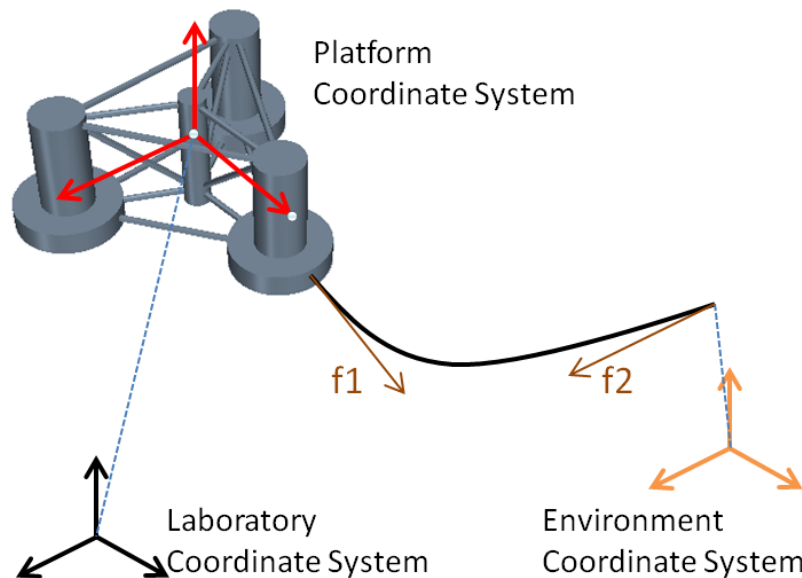

Fig 3-5. Mooring line system

In addition, a wave-damping area was applied, considering wave reflection near the outlet boundary; this treatment includes a wave-damping zone. The wave-damping area was designed to minimize the effects of wave reflections on the far downstream outlet boundary. As a result, the VOF wave could be damped in the pressure outlet boundary to reduce wave oscillations. This damping introduces vertical resistance to the vertical motion of the wave. A VOF wave damping boundary option node is added to the physics conditions for each boundary in the region. The distance from the VOF wave damping-enabled boundary at the damping starts. The specified value of wave damping length has been set 80m. As Fig 3-6 shown.
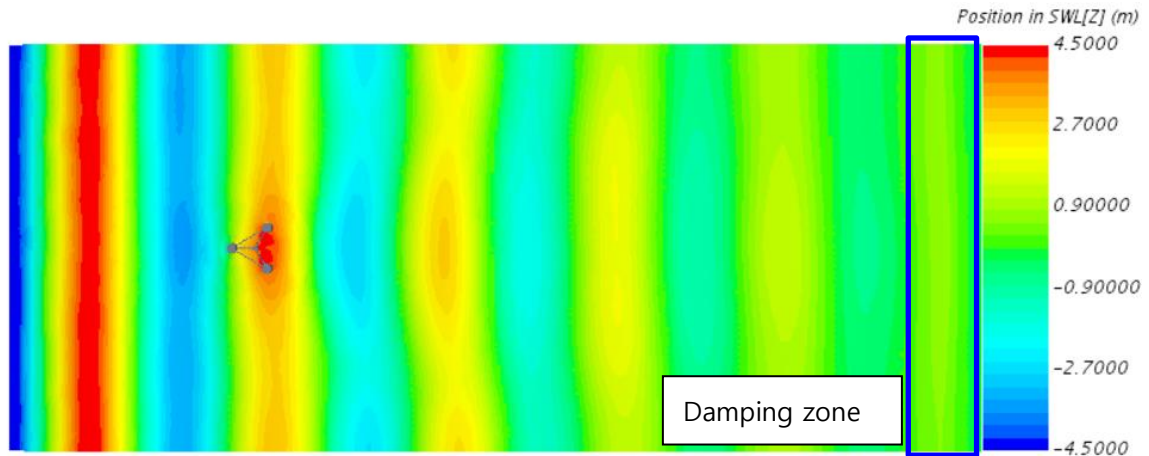
Fig 3-6. Damping zone in wave test

The damping zone, which also called sponge layer, takes effect by adding one additional artificial viscous term as a source term to the momentum equation. The new term is thus expressed as:

$$f_s = -\rho \mu_s U \tag{3.12}$$

Where μ_s is the artificial viscosity calculated by the following equation:

$$\mu_s(x) = \begin{cases} \alpha_s \left(\dfrac{x - x_0}{L_s}\right)^2, & x > x_0 \\ 0, & x \leq x_0 \end{cases} \tag{3.13}$$

In which α_s defines the damping strength for the sponge layer; x denotes the coordinates of the grid cells in the x direction; x_0 and L_s represent the start position and length of the sponge layer. The artificial viscous term is only effective for those cells inside the sponge layer and is equal to zero elsewhere.

IV. Aerodynamic validation of wind turbine

4.1 Numerical setting and mesh convergence test

An aerodynamic simulation of the rotor part was performed to validate the accuracy of the 3D modeling and numerical modeling setting with the CFD method. The hexahedral computation domain size and boundary type is 8D(x) × 5D(y) × 3D(z) and extends up to 2.5D and 5.5D in the upstream and downstream x-directions from the wind turbine, respectively.
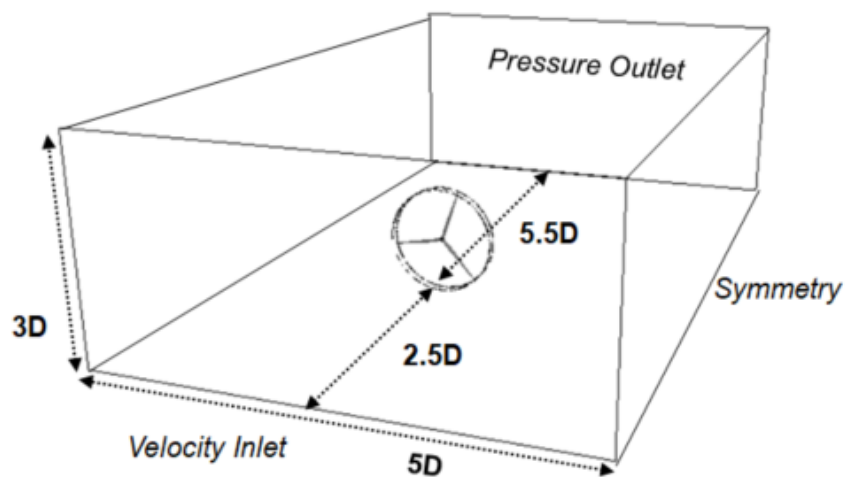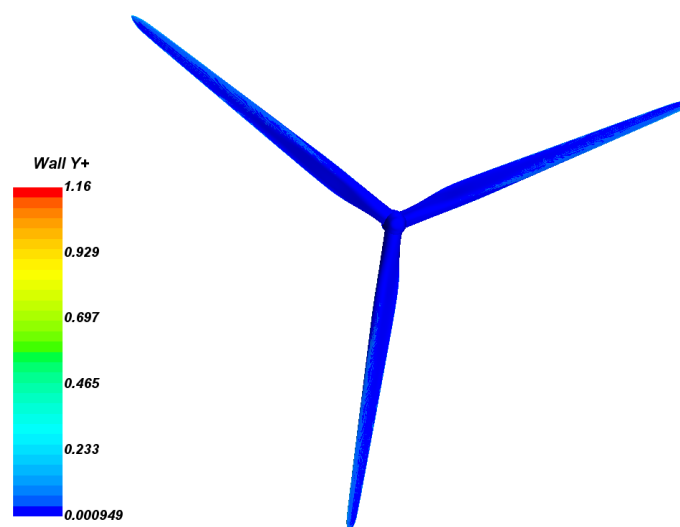

Fig 4-1. Fluid domain of rotor

Fig 4-2. Y plus distribution of rotor

- 29 -

Both poly grids and trim grids were tried in the mesh test procedure, and the trim mesh was finally selected owing to its robust features and relatively low computation cost. Nineteen layers of prism grids were generated to determine the blade-attached flow, and the near-wall first boundary layer thickness was 3.82×10^{-6} m. A mesh convergence test was also performed, and the results are given in Table 5; four sets of grids were generated to with different grid densities while all the other parameters remained unchanged, and 22 million grids were selected with both a short calculation time and acceptable power loss. Details of the trim mesh around the blade tip are presented in Figure 4; at the same time, denser grids around the leading and trailing edges of the airfoils were used to detect fluid details. Y plus is a dimensionless value used to measure the mesh quality; a value below 1 is produced when the k-ω SST turbulence model is applied. In this study, the Y plus value was much lower than 1 in all five cases.

Table 4-1. Mesh convergence test

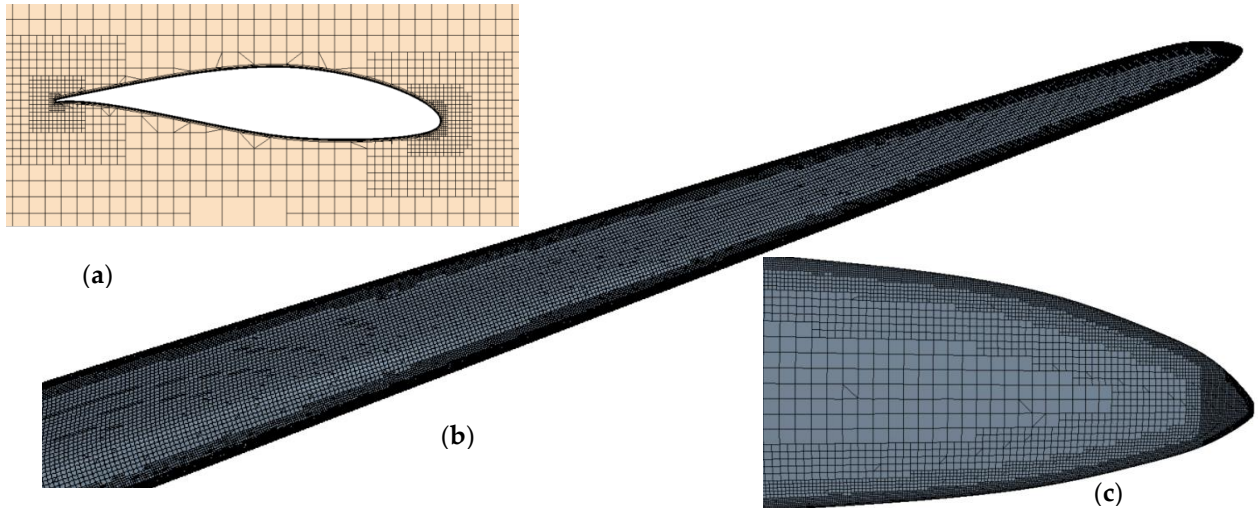| Mesh	Thrust(kN)	Power(kW)	Power Variation
14 millions	726	4980	-5.5%
22 millions	731	5090	-3.4%
30 millions	729	5107	-3.1%
38 millions	734	5270	0%

Fig 4-3. Trim cell detail: (**a**) Mesh section near 45m spin wise airfoil; (**b**) Trim mesh around blade tip; (**c**) Blade surface mesh

4.2 Rotor aerodynamic performance validation

Currently, there are three main methods used for simulating aerodynamic performance: the BEM method, GDW model, and CFD model. The results of each model are shown in Figure 5. The CFD results are in good agreement with those of the other codes with regard to both power and thrust prediction, which were collected by GNU using FAST code. The BEM method was observed to overestimate results at a relatively high wind speed, which is also noted in other studies [20]. Sivalingam et al. also compared results between the CFD and BEM methods; there was good agreement in terms of the thrust and torque results below the rated speed. However, because of tip loss factors at relatively high wind speeds, a deviation of axial induction factors was shown by the BEM method, while the CFD method captured wake rotation accurately [21].
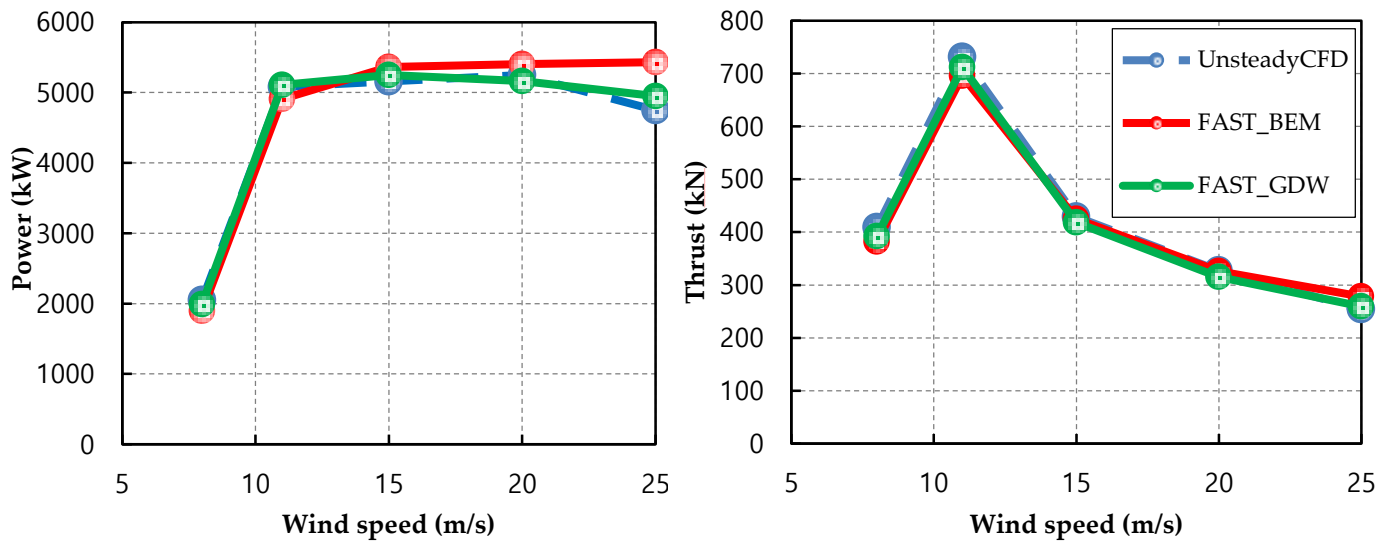
Fig 4-4. Power and thrust in 8m/s, 11m/s, 15m/s, 20m/s, 25m/s uniform wind speed

At present, the two most commonly used methods to deal with blade rotation are MRF method and RBM method. However, MRF method can only get steady result which unable to deal with the unsteady situation, here we use RBM method to deal with the rotation of grid near the blade: to be specifically, the whole computational domain is divided into two sub-domains. The grid surrounding the blade region moves with the blade and keeps relative static with the blade, while the other region keep stationary state. The information in flow field such as gravity element of the two regions are achieved by interpolation with percentage weights at the slip interface, where the weights are determined by the proportion of the overlapping regions of the stationary and dynamic surfaces as Fig 4-5 shown. The RBM method is different from the moving grid method, compared with the moving grid method, it only needs to deal with the whole motion of the local grid and the interpolation of the interface. It does not involve the deformation and remesh of the grid, thus saves the computing time and computer memory. Therefore, it is widely used in the engineering calculation of rotating motion.
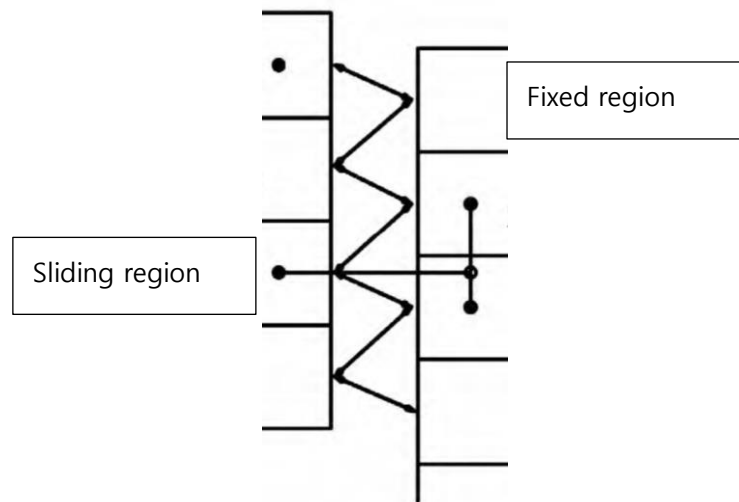
Fig 4-5. Interface of sliding mesh

Simulation in this study obtained numerical results considering rotating motion of wind turbine blades. Considering the whole motion of the slip surface mesh, the time step cannot be too large. In order to save calculation time and obtain the convergent and stable results, the average values of the last few cycles of rotation are selected as the wind turbine average thrust and torque.

According to the variation of incoming wind speed, NREL 5MW wind turbine also rotate with different speed. Here, two low wind speed conditions, one rated wind speed and two high wind speed conditions were simulated respectively. Firstly, we applied moving reference faction (MRF) method to carry out steady-state simulation. When the residual reached 10e-4 and the aerodynamic loads changed less, the fluid domain was considered reliable and stable. The transient calculation is carried out on the basis of steady state calculation using RBM method. When the blades rotate for 4 turns, the thrust and torque are basically stable. When the incoming flow just passes through the wind turbine, the vortex behind the blades can be observed obviously, with the increasing of flow distance, the vortex gradually disappears. The above values obtained by CFD were compared with the BEM results, the CFD simulation results were smaller than BEM results. When in low speed conditions, the difference is very small, but when the wind speed is higher than rated wind speed, the deviation gets large. This is mainly because the flow field at the airfoil section in

- 33 -

the middle of the blade gradually in the dynamic stall state in relative high wind speeds.

For the power curve, the result agrees well in low wind speed, however, the deviation increases gradually when the wind speed higher than the rated wind speed, this is because the angle of attack at the blade element section is smaller and the flow adhesion with blade, which means the flow along the wing-span direction is smaller, so the stall effect can be neglected. The calculated results are in good agreement with different codes. However, when the wind speed increases gradually, especially when the wind speed is greater than the rated wind speed, the phenomenon of dynamic stall in blade part becomes serious. At the same time, due to the rotation of wind turbine, the airflow flowing along the wing-span direction and the total deviation increases. Further, with thrust curve shows, when the wind speed lower than the rated wind speed, the horizontal thrust of the wind turbine increases with the increase of wind speed, reaches the peak near the rated wind speed, and when the wind speed is higher than the rated wind speed, the horizontal thrust of the wind turbine decreases with the increase of wind speed, which is also approximately regarded as a linear change. The decrease of thrust is due to the pitch control system of the wind turbine.

In blade element theory, we assume that only a single blade element is chosen to analyze. The force acting on the blade element under the wind load is on the 2D plane. There is no flow in the blade wing-span direction, and the air pressure in the blade wing-span is basically unchanged. Therefore, when the pressure gradient in wing-span is very large, the accuracy of blade element theory will decrease. In BEM theory, the same assumption is adopted as in blade element theory, that is, only a single section of blade is considered, so the lift-drag coefficient is obtained from the 2D plane experiment, but when the incoming wind speed is high, still use 2D plane experiment data lead to lower value in BEM theory compare to actual measured value. Further, in practice the wind turbine is three-dimensional, and the rotation of the blade will cause the flow on the blade surface to flow along the outer surface of the blade wing-span direction. At the same time, due to the acceleration of Coriolis force, the air flow speed alone the blade chord direction will increase. These two reasons together lead to the stall critical point of the blade moves towards the tip direction. Compared with the 2D case, the aerodynamic performance of the blade is

obviously different, that is, the lift-drag coefficient is quite different from the experimental data. In this case, the stall AoA of section will increase, lift coefficient also increase and drag force decrease. This phenomenon is more obvious near the root of blade.

4.3 Study of wind profile and tower dam effect under onshore WTG conditions

The aerodynamics of the NREL 5-MW fixed wind turbine was studied on the full scale without the floating platform and the results will later be compared with the data for a floating wind turbine. All the numerical settings used in the CFD-rigid body motion (RBM) approach in the previous simulations applied to the rotor part, except the inlet uniform wind speed were respected to wind profile. As Fig 4-6 shown.
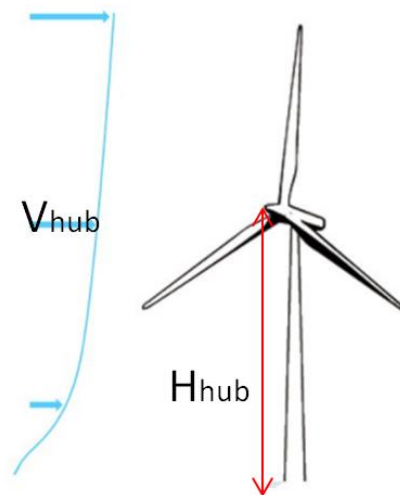

Fig 4-6. Wind profile

The wind profile shows variations in the horizontal wind speed with height, which may result in increased fatigue loading and reduced power output, usually characterized by the power law, as follows:

$$v = v_{hub}(H/H_{hub})^{\alpha} \tag{4.1}$$

Here, v means income speed at any height, v_{hub} means income speed at hub height, H_{hub} means height from hub to ground, the wind shear exponent (alpha) was 0.12 for flat onshore conditions. Fig 4-7 illustrates wind profile applied in fluid domain.
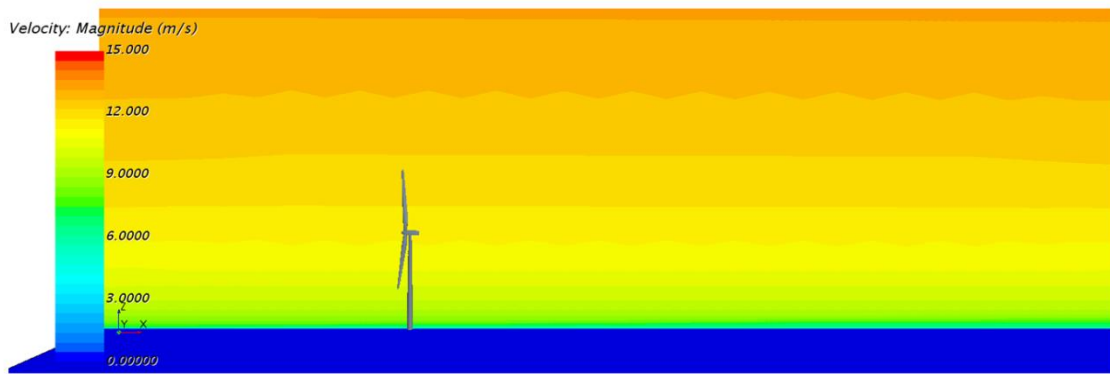
- 35 -

Fig 4-7. Wind speed distribution in fluid domain

Besides, Figure 6 illustrates the computational mesh domain; the upstream boundary of the inlet is defined as velocity inlet, and the pressure outlet is defined as the downstream boundary. Symmetric boundary conditions were applied in far field region and a no slip wall condition was imposed on the surface. Tran et al. [20] had carried out a convergence test to determine the fluid domain size; herein we used a hexahedral computational domain size of 1000 × 600 × 275 (Length, Width, Height), the same as that in Tran et al, in the x-direction; the fluid domain extended 313 m upstream and 687 m downstream to help analyze the fluid domain and consider the impact of the vortex after the tower, considering the time-dependent motion of the rotating blades; we used the RBM method in this study.
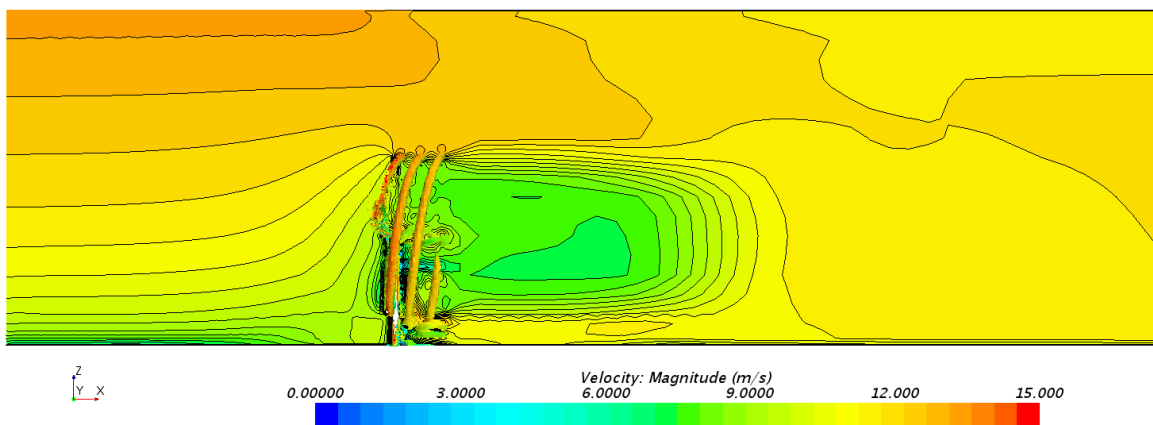

Fig 4-8. Onshore 5MW wind turbine fluid domain

Aerodynamic simulations of onshore wind turbines were conducted using the RBM method under unsteady conditions; the obtained torque output under 11 m/s wind

- 36 -

conditions was compared with the results of the FSI method obtained at the University of California. As shown in Fig 4-9, there was good agreement between both, but the predictions from our simulation were slightly higher, which may be because blade deformation was ignored in the RBM method [22] [23]. Power and thrust in other wind condition have also been simulated, pitch control system works after rated wind speed arrive, in order to keep stable power production, pitch angles also been summarize in the Table 4-2.
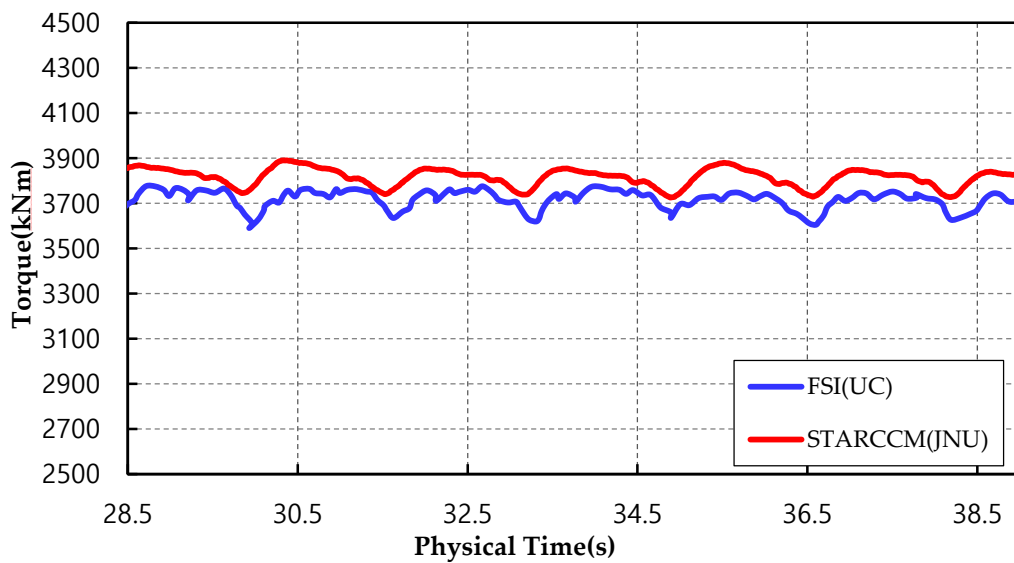

Fig 4-9. Torque curve between FSI method and unsteady method in 11m/s wind speed

Table 4-2. Aerodynamic performance of 5MW onshore wind turbine in different wind speeds

Speed (m/s)	Blade Pitch (deg)	Rotating Speed (rpm)	Thrust (kN)	Power (kW)
8	0	9.16	389.9	1859.3
11	0	11.89	696.5	4617.8
15	10.45	12.1	396.0	4635.6
20	17.47	12.1	300.7	4759.8
25	23.47	12.1	234.0	4129.2

V. Hydrodynamic response of floating platform

5.1 Description of floating condition

The bottom of the tower of onshore wind turbines is usually installed on the base of the ground, which is rigidly connected by bolts. The deformation and displacement of the tower can be neglected considering wind load. There is no relative movement between the wind turbine and the incoming wind. At present, the so called offshore wind turbine near coast are basically same with onshore wind turbine, although the part under the sea is affected by wave loads, the displacement of the tower is small enough to be ignored. With the development of technoledge, the floating platform structure was adopted. The platform is connected and fixed with the bottom of the seabed through mooring lines. Part above sea surface of FOWT is affected by the wind load, part below water surface is affected by the wave load, those two force combine together and lead to large movement to FOWT, as a result have a significant impact on the relative velocity inevitably. The motion will also cause continuous changes of azimuth angle between FOWT and incoming wind, which will affect the aerodynamic performance of the wind turbine. In couple effect of wind, wave, current, six degree of freedoms movement will happen. The six kinds of motion are surge, sway and heave in translating motion, compared with the coordinate system fixed at the center of wind turbine, FOWT also rotate around the axis, there are yaw, pitch and roll respectively.
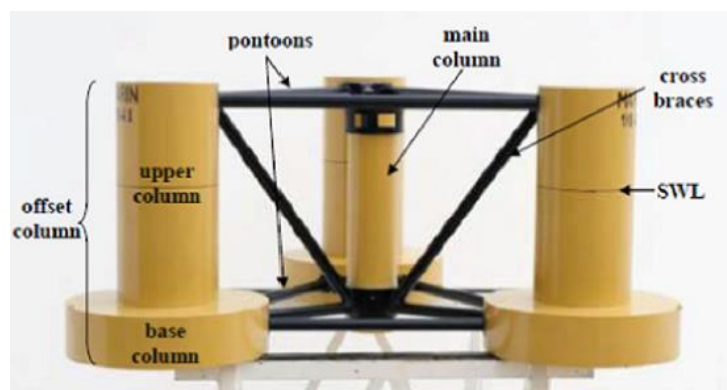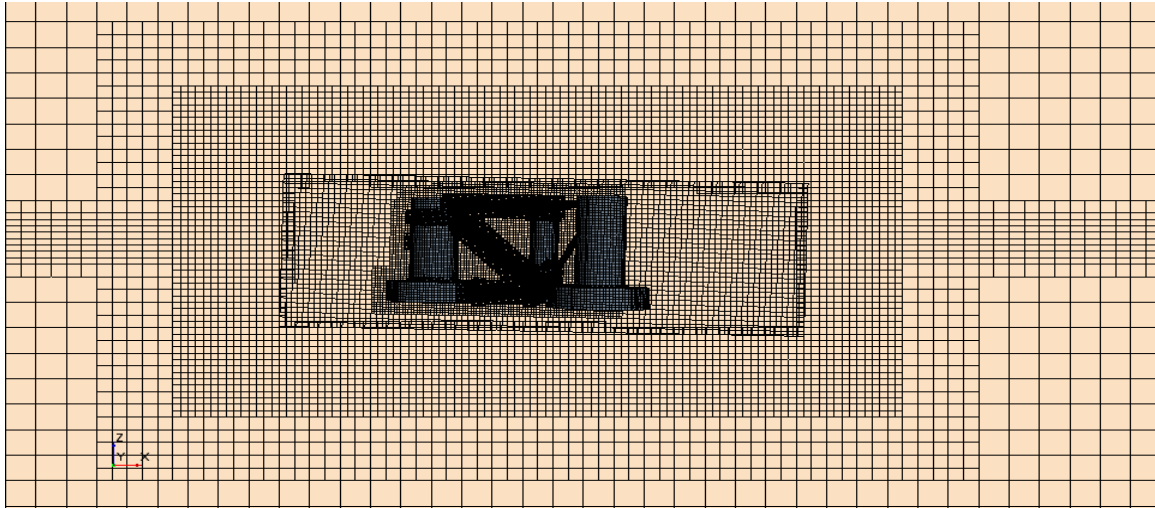

Fig 5-1. Semi-submersible platform in MARIN wave tank

5.2 Free decay test

The full-scale OC5 semi-submersible platform has been modeled and simulated to investigate hydrodynamic response, by DFBI method and overset mesh techno ledge. In order to reduce total mesh in this simulation and accelerate simulation speed, also considered minor effect of air flow to hydrodynamic response, only platform and mooring line system are considered. In this study, we applied a hexahedral fluid domain with dimension of 1200m in X direction, extend 300m in upstream and 900m in downstream direction, respectively. The weith of two symmetry boundary is 500m, and the fluid domain height is 300m, platform is set 200m above seabed and 100m from upper boundary, respectively. Becase of robust and high-quality features of trim grids, trim grids were used in both outer fluid domain and inner overset mesh domain. To better catch fluid detail, we used denser mesh around platform and water surface；we generated 8 layers of prism grids, with progression factor of 1.2, and total prism thickness of 20 cm. Mesh refinement near water surface set grid size in x and y direction 4m, this size is about 1/80 about wave length, grid size in z direction set 1/160 of wave length, which is 2m. Details of platform mesh are shown in Fig 5-2.
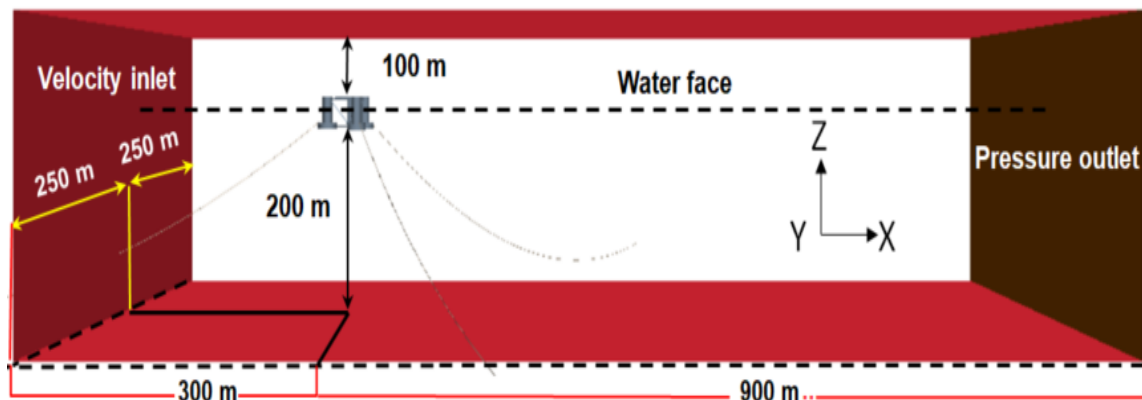
(a)

(**b**)

Fig 5-2. Free-decay test mesh domain: (**a**) Overall view; (**b**) Detail view

Free-decay tests are methods generally used in a wave tank to determine the natural period of a floating system. The OC4 project was based on a 1/50th-scale semi-submersible platform in the MARIN wave basin in 2011. This model was revised two years later, to provide more precise test data for the OC5 project [18]. Owing to the different properties of the mooring line (line stiffness) and rotating inertia forces in the two tests, the OC4 and OC5 data reveal good agreement in terms of translation motions (surge, sway, and heave) but a relatively large discrepancy in terms of rotating motions (roll, pitch, and yaw), as observed in Table 6. 6-DOF free decay tests were conducted to determine the hydrodynamic damping characteristics of the OC5 semi-submersible platform. The wave mode was set as still water, and the air density was zero. Only the platform was considered to simplify the simulation, but the gross mass should also be considered. The platform was given a prescribed displacement and released to move freely from the initial position. This test considered only three rigid-body DOFs, that is, the surge, pitch and heave motions.

Table 5-1. Natural period in OC4&OC5 project

DOF	OC5 natural period	OC4 natural period
Surge	107s	107s
Sway	112s	112s

Heave	17.5s	17.5s
Roll	32.8s	26.9s
Pitch	32.5s	26.8s
Yaw	80.8s	82.3s

The results are presented in Figure 8, along with the simulation results from GNU and the wave basin test results from phase II of the OC5 project. The heave and surge time-domain responses for the platforms are in good agreement, because similar results were obtained in the heave and surge periods in the OC4 and OC5 projects. However, in case of pitch, a relatively large discrepancy was observed in the time-domain response for the GNU simulation. As mentioned above, this effect may be owing to the different properties of the mooring line and rotating inertia forces of the platforms used in the two projects. Based on the natural period of the pitch, the pitch results were in good agreement with the OC5 test data.
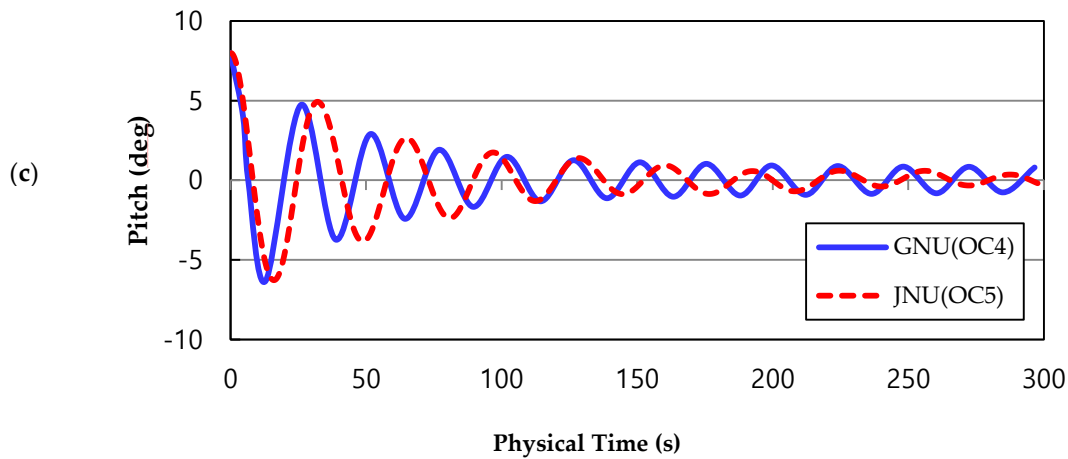
(a)

(b)
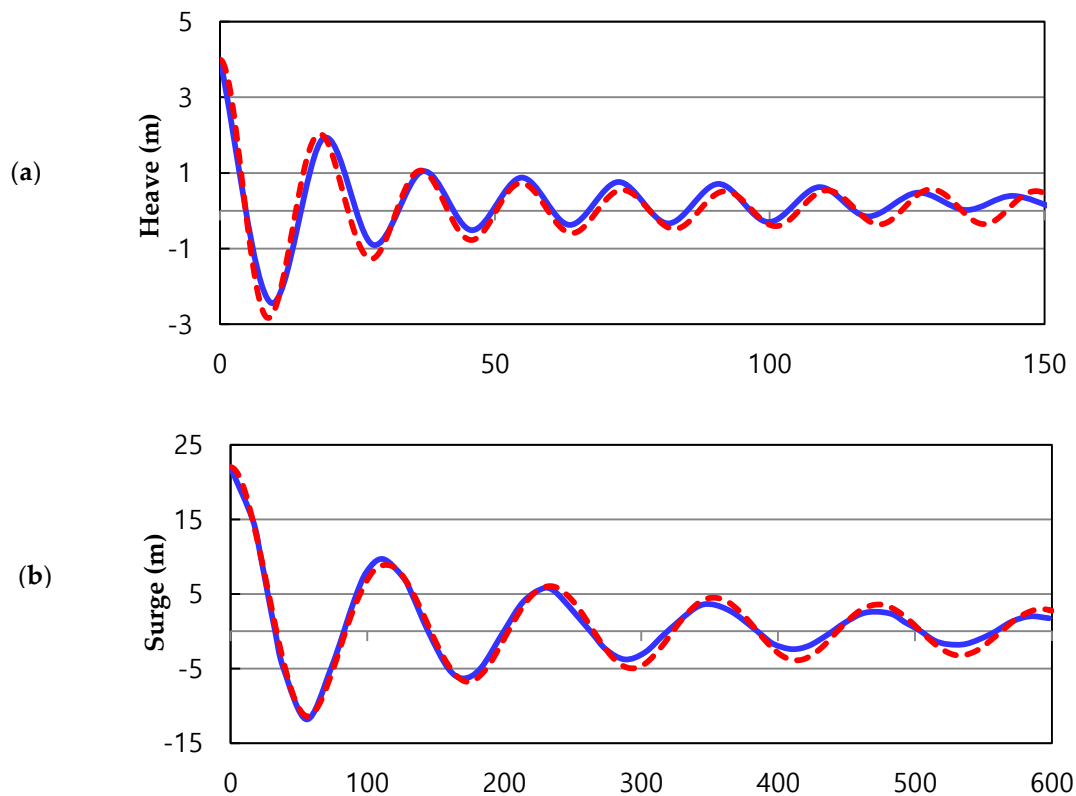
Fig 5-3. 3-DOF movement of platform by time domain: (**a**) Heave movement; (**b**) Surge movement;(**c**) Pitch movement

5.3 Hydrodynamic response under regular waves

The FOWT system's hydrodynamic response also simulated under regular wave condition in this study, considering little effects of wind compared with wave, usually aerodynamic forces were assumed not exist in other studies and upper part above platform not modelled.

The characteristics of the DeepCWind platform in the presence of regular waves was investigated by the calculating of the response amplitude operators (RAOs). An RAO is the normalized value of the amplitude of a periodic response of a field variable by the amplitude of a regular wave. The platform was initialized at a static position and a regular wave was introduced. The regular wave under study had a wave amplitude of 3.79 m and a wave period of 14.3 s. sever time-step have been applied to obtain a both accurate and less computation cost result, at last, we applied 0.0056 s which can efficiently show an optimum value. Fifth order wave applied in regular wave test, here, a fifth order wave is modeled with a fifth order approximation to the Stokes theory of waves. This wave more closely resembles a real wave than one generated by the first order method. The transient start-up period should not be considered in the results. After simulation runs for 600 s, the platform movement achieved a nearly periodic quasi-steady state. The surge, heave, and pitch motion amplitudes were calculated by averaging the amplitudes over the last 8 wave periods [16],

- 42 -

These values were then normalized using the amplitude of the regular wave to obtain the RAO. The amplitude dynamic response of pitch, heave and surge simulated 600s can be observed in Figure.
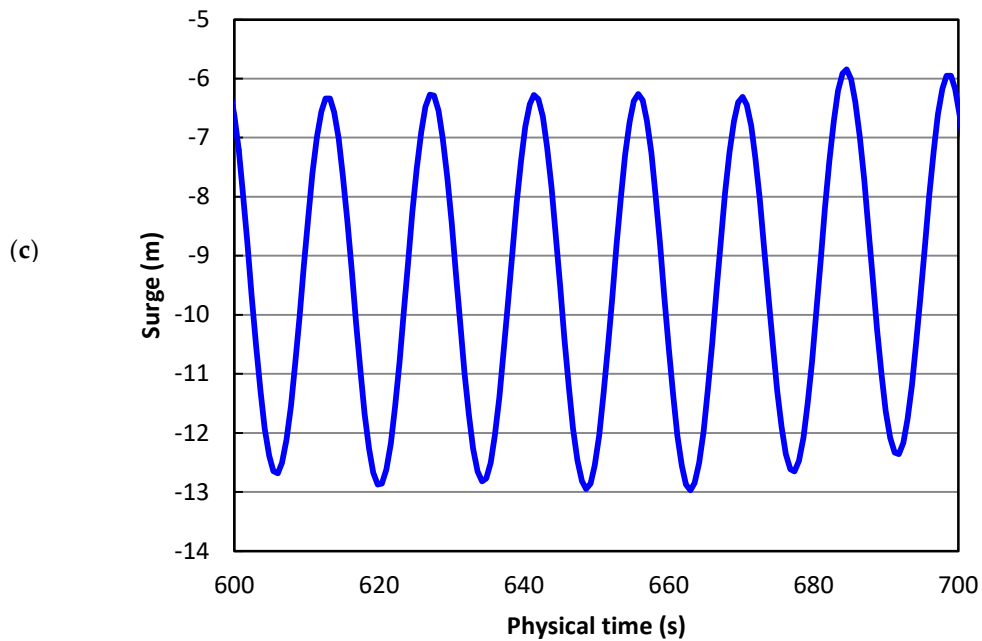
(a)

(b)
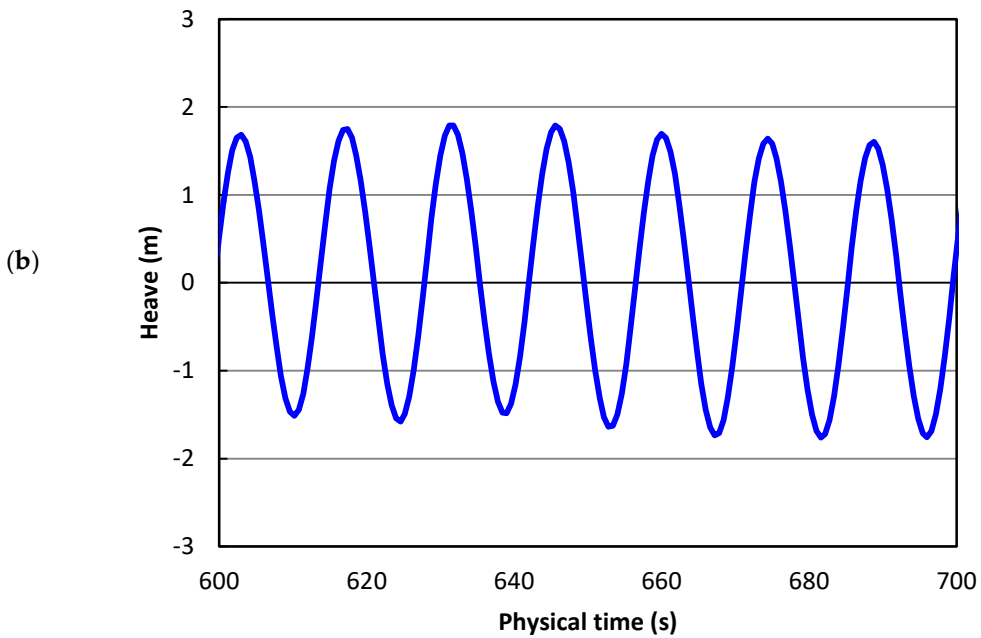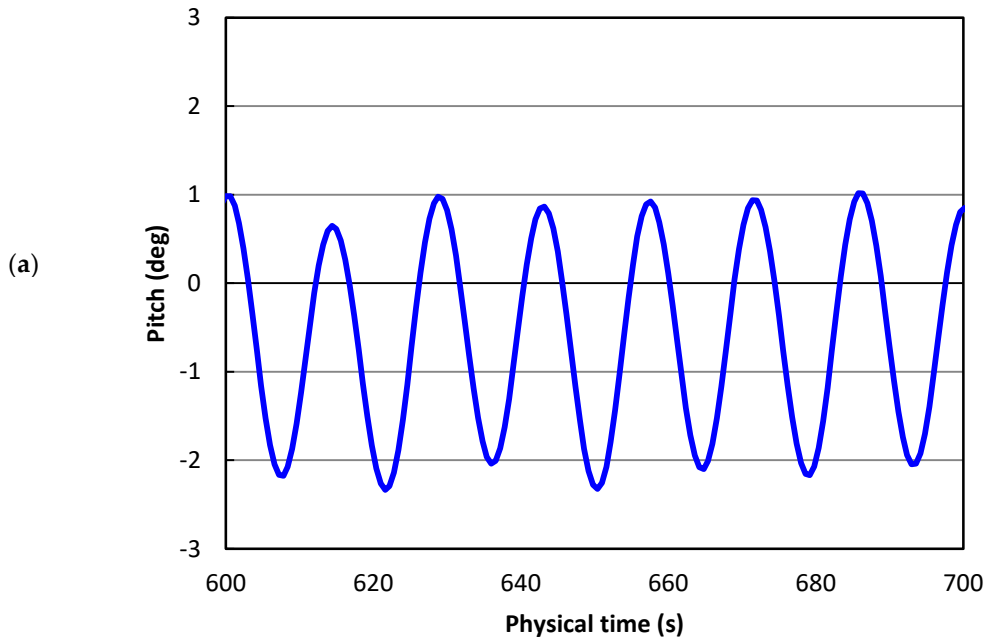
Fig 5-4. 3-DOF movement of platform in regular wave condition: (**a**) Pitch movement; (**b**) Heave movement; (**c**) Surge movement

   Figure shows the wave effect to OC5 semi-submersible platform, here we used the mentioned wave data, with no wind and current conditions. The wave surface elevation contours show wave run-up effect on platform upper column, this detail can also be detached by a post-process during a wave period. Here the wave length we applied (230m) is much larger than platform dimension, as a result the platform tends to be impacted during the crest period of wave elevation, the contour also indicates as a numerical tool, unsteady CFD method can well describe physical hydrodynamic detail, as wave run-up effect and so on. Further more, unsteady pressure distribution also be simulated by this study so that one can conduct definite structural analysis in the design process of an semi-submersible platform, complex physical flows around it can visualized in this study.
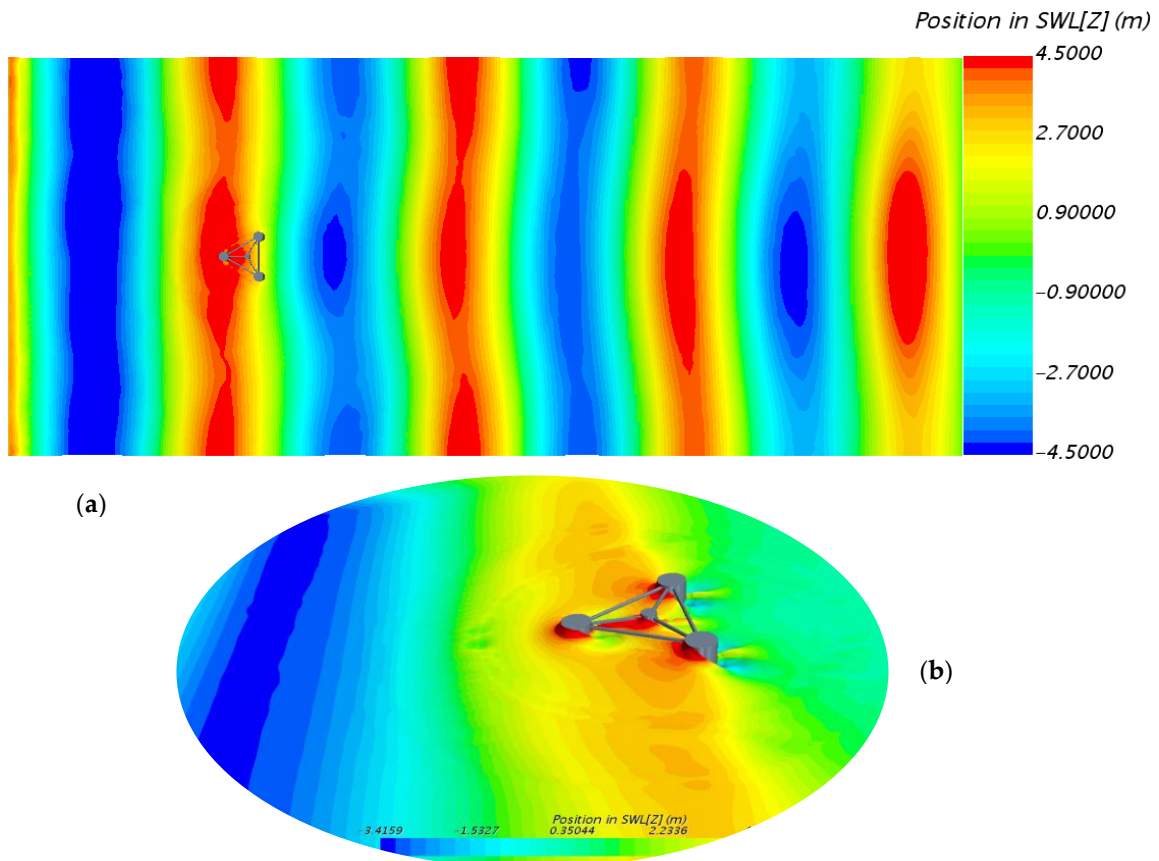
Position in SWL[Z] (m)

Fig 5-5. Wave in fluid domain: (**a**) Wave elevation in whole domain; (**b**) Wave detail near platform

The RAOs of Phase II of the OC5 project were higher for the surge, heave, and pitch DOFs, similar to our simulation results obtained using the unsteady CFD method, as shown in Fig 5-6. The comparison between present study and CFD from other institutions show good agreement in surge and heave, the discrepancy of pitch might result from difference in OC5 mooring line and indicate that a more accurate mooring line system should be adopted in future study. Because large discrepancy in hydrodynamic response can lead to critical effect in whole FOWT system. In additions, some discrepancy between scale model in wave basin and full model with CFD method can be also observed, this because CFD method cannot predict friction force between mooring lines and sea bed, neither the interaction between mooring lines and hydrodynamic loads. However, compare with other numerical codes, the unsteady CFD method is accurate enough to simultaneously consider all physical flow, such as viscous damping, vortex shedding, run-up wave and flow-induced interaction.
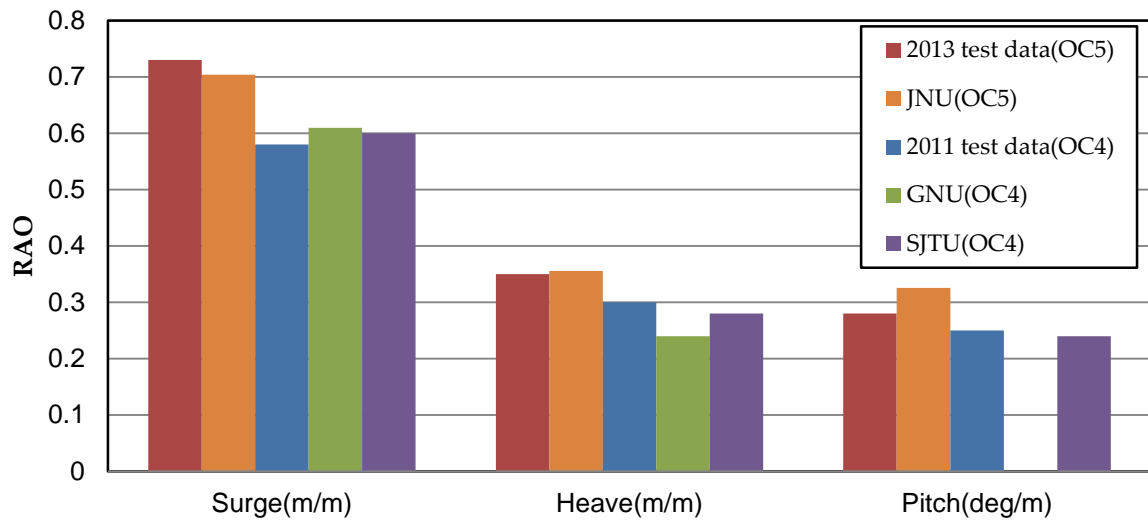
- 45 -

Fig 5-6. Comparison of RAOs for surge, heave and pitch

VI. Full coupled wind-wave simulation

The full-scale DeepCwind OC5 model in a coupled wind-wave excitation condition was finally conducted using the DFBI method mentioned above. Figure 10 shows the fluid domain, together with an x-z plane section of the mesh distribution in the whole fluid domain. To obtain the fluid details near the free surface, as well as those near the turbine blade tip and vortex regions after the tower, mesh refinement was performed around the blades and platform, as shown in Figure 11. Nearly 27 million cells were generated using the built-in trim mesh feature in STAR-CCM+.
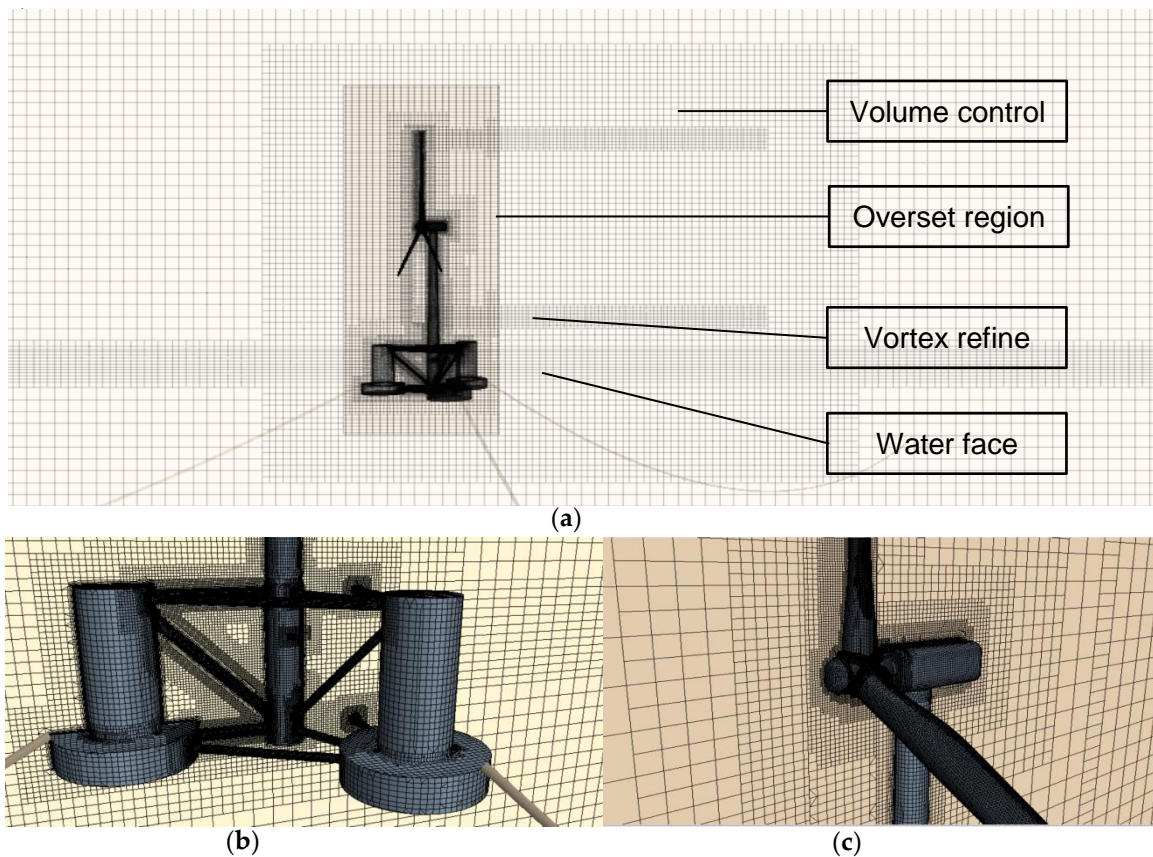

Fig 6-1. Full-coupled FOWT domain: (**a**) Mesh distribution in x-z plane; (**b**) Close-up view of mesh around platform; (**c**) Close-up view of mesh around wind turbine

The wind speed V was assumed to be the rated wind speed (11.4 m/s); the wave height and wave period were assumed to be 7.58 m and 12.1 s, respectively, similar to the MARIN

제주대학교 중앙도서관
JEJU NATIONAL UNIVERSITY LIBRARY

wave basin. After a 10 s start-up time, the aerodynamic output for wind turbine was stabilized and the platform was released to move. A computational flow chart for the FOWT is presented in Figure 12. The time for one revolution of the blades with a rotation speed of 12.1 rpm is 4.96 s. The time-step size (dt) of 0.07009 s utilized here corresponds to a 5° increment in the azimuth angle of the blade for each time-step. The wave heading angle is 0° and wave parallel the direction of mooring line 2, which is also parallel to the platform surge direction. All the computations of the FOWT considering the wind-wave coupling were performed using a 4U multi D500 server. The elapsed real CPU time for parallel processing per time-step with 15 sub-iterations was 6 min when using 66 CPUs. The total number of iterations for a simulation run time of 300 s was approximately 30000. The total simulation time to obtain results using 66 CPUs was 20 days.
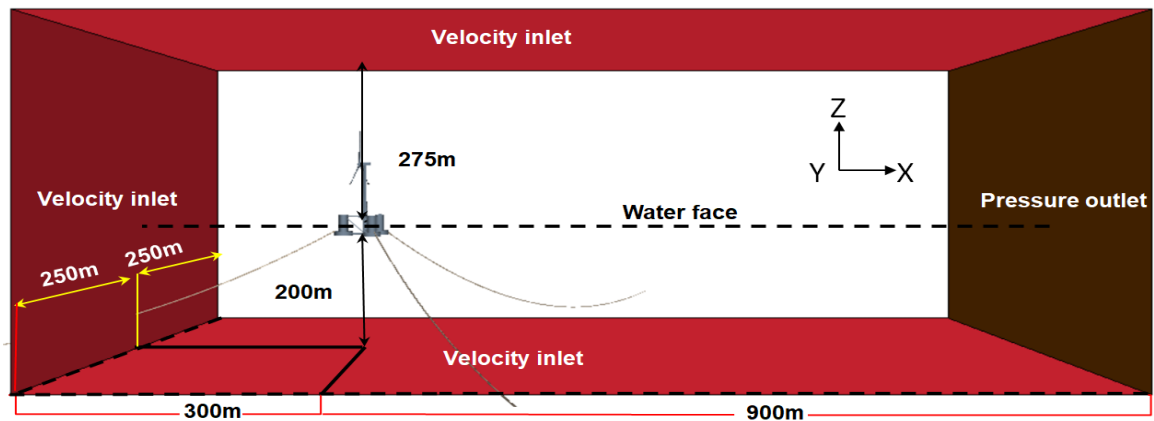

Fig 6-2. Full-coupled FOWT domain fluid domain size and boundary conditions

Figure 13 demonstrates the vortex contours with 0.5 Q-criteria, colored according to the velocity magnitude component, where the free surface is colored according to the surface elevation. After post-processing, as easily observed in the figure, strong vortices appear in near the blade tips and roots. The presence of the tower caused a complex flow wake because of the interaction between the tower and flow. Such a detailed flow map is useful to identify the means for improving the wind turbine power output in the design stage. This is an advantage of the CFD method, which is not present in other codes such as FAST. The size of the vortex tubes gradually decreases with time, and the patterns can be described by an iso-vorticity value.
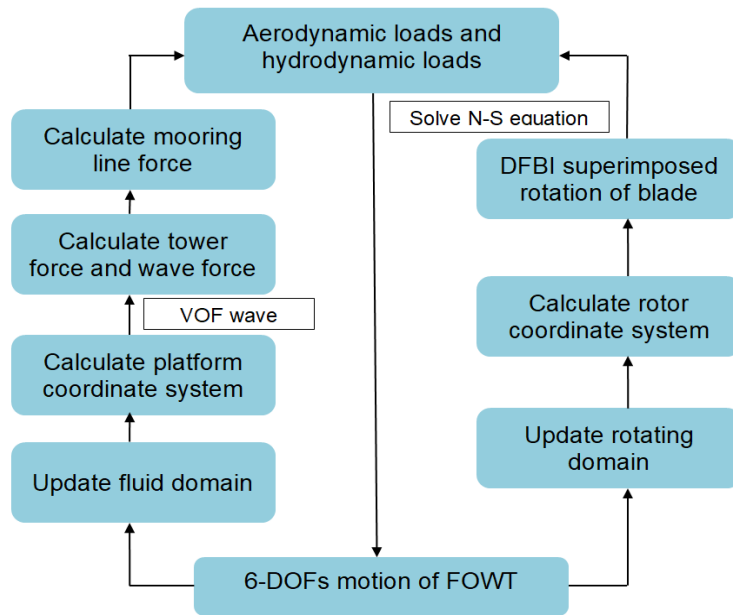
Fig 6-3. Flow chart of fully coupled simulation in wind-wave condition

Herein, one wave period is separated into eight steps, i.e., T1 to T8; the duration from T1 to T8 represents one period of the platform surge motion. When the wind turbine moves backward, the number of vortex tubes increases, and the gaps between the blade tip vortices tend to continuously decrease at the same time. Figure 14 shows the fluid field and turbulence wakes between the fluid and tower and nacelle during the platform surge motion at different times. It shows that the generated vortexes near the tower and nacelle configurations diffuse outward as the platform moves backward, and vice versa.
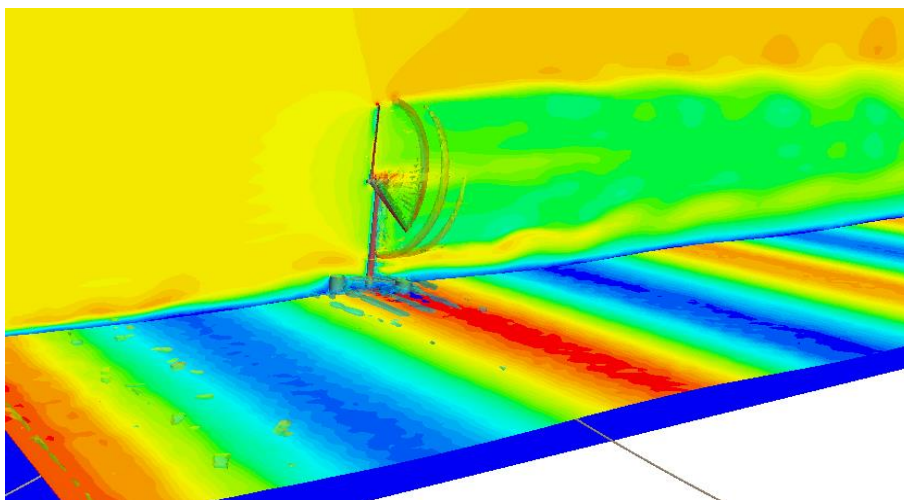

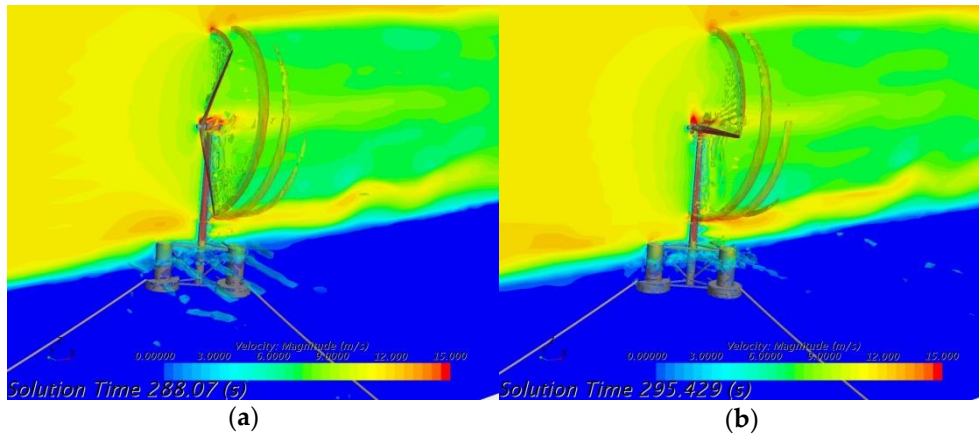**Fig 6-4.** Velocity scene and water elevation

Fig 6-5. Instantaneous iso-velocity contours within one period: (**a**) Upwind direction movement; (**b**) Downwind direction movement

The RAOs of surge, heave, and pitch in the full-coupled configuration under wind-wave excitation conditions are given in Table 7. Compared to the result of the regular wave test, where only regular waves exist, under a no wind condition, some discrepancies can be observed. The motion RAOs and the time-average values over the last four wave periods for 3-DOFs were compared. Because of the unavailability of MARIN test data for the wind and wave conditions simulated herein, the comparison was only performed with the result from a previous study. All the 3-DOFs, i.e., heave, surge and pitch showed small amplitudes compared to the results of the regular wave test without wind conditions. The incoming wind from the x direction obviously has a significant effect on the restoring force of the mooring line; hence, the FOWT system cannot be restored to the equilibrium position as in the regular wave test. The incoming wind increased the aerodynamic thrust towards floating system and pushed platform further away in backward direction, also leading to an increase in the mean surge. Nevertheless, the close agreement between the results for the 3-DOFs demonstrates the capability of this method.
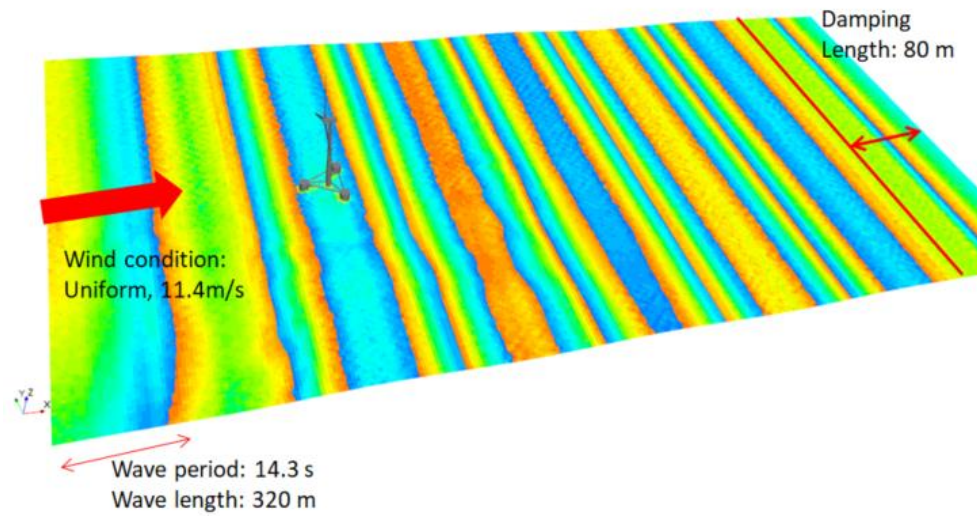
**Fig 6-6.** Aero-hydro condition of full configuration simulation

Table 6-1. Motion RAOs in different environmental conditions

Motion	Wave only	Wind-wave coupled
Surge(m/m)	0.70	0.12
Heave(m/m)	0.36	0.13
Pitch(deg/m)	0.33	0.07

Table 6-2. Dynamic response of FOWT in wind-wave condition

	Parameters	Value
Power output	Range (kW)	3446-4689
	Mean value (kW)	4181
Thrust force	Range (kN)	759-838
	Mean value (kN)	801
Pitch angle	Range (deg)	4.5-5.3
	Mean value (deg)	4.9
Surge motion	Range (m)	7.9-9.8
	Mean value (m)	9.1
Heave motion	Range (m)	-0.7-0.7
	Mean value (m)	0.1

Thrust and power are two critical aerodynamic performance factors for evaluating a wind turbine. Thrust is defined as the integrated force component normal to the rotor plane. The power output and thrust force time-histories for the coupled simulation are presented in Figure 15 along with the dynamic responses of the pitch motion rate of the platform. The response curves for power and thrust act at the same frequency as the incident wave. Owing to the tower shade effect, the curves for power and thrust force exhibit periodical fluctuations with a period of 120° for the blade rotation. However, the effect of the tower dam on the power output of the wind turbine is less than 5%. In addition, the variation in pitch motion also acts at the same frequency as the inlet wave. When the platform moves in the upwind direction, the power output and thrust force both increase, while the aerodynamic load decreases as the sign of the pitch motion changes. This is because the upwind pitch motion of the FOWT increases the relative velocity between the wind turbine and inlet wind, and the angle of attack for each blade section increases correspondingly.
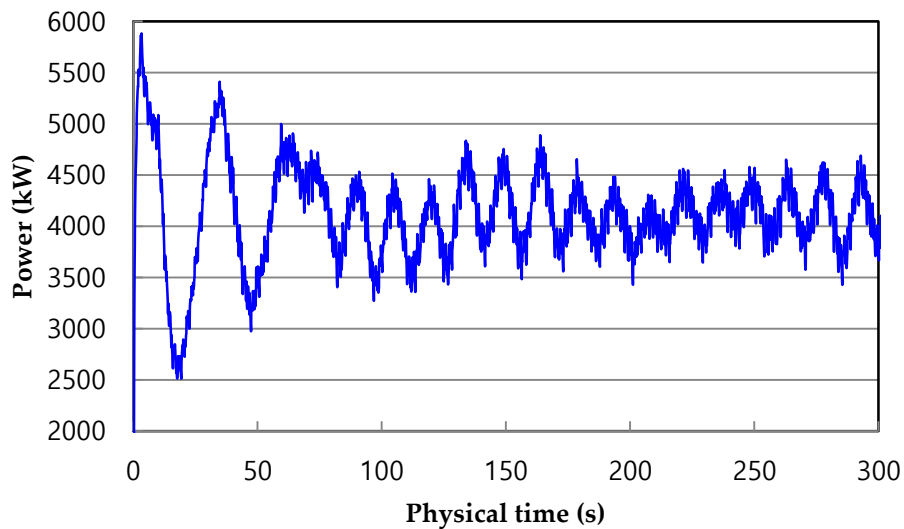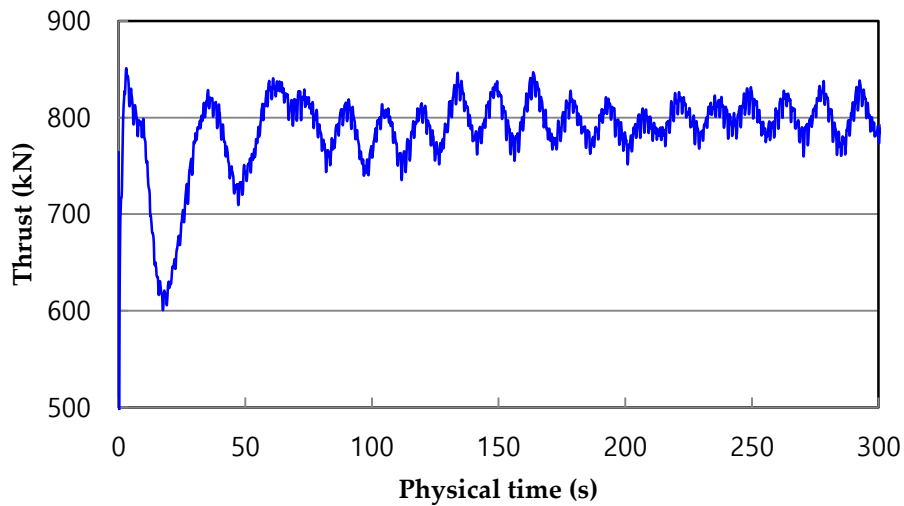
Fig 6-7. Fully- coupled FOWT aerodynamic performance

The dynamic responses of the wind turbine and typical platform motions after 300 s of simulation are presented in Table 8. The power output varies from 3446 kW to 4698 kW at the rated wind speed. The variation in power is larger than that in the thrust force; that is, the power output is more sensitive than the thrust force to platform motion. Then aerodynamic performances of the onshore fixed wind turbine and offshore floating wind turbine were compared and the average thrust value was calculated over the last 4 periods. In case of thrust, a 7.8% increase was observed in floating offshore turbine, the floating offshore wind turbine had an average thrust around 796kN and the onshore wind turbine had an average thrust of 738kN, which indicating a relatively small load on the hub and blades. This is because of the thrust force acting on the top of the tower, as a result of which the platform always moves in the upwind direction to offset the capsizing moment induced by the thrust force. In the case of the power curve, the average power value was calculated over the last 4 periods. A 10% decrease was observed in floating offshore wind turbine, which is likely due to the smaller project area and relative income wind speed when the platform pitches, as shown in Figure 16. Accordingly, the platform surges from 7.9m to 9.8m, which is also due to the thrust force that has to be offset by the mooring line tension.
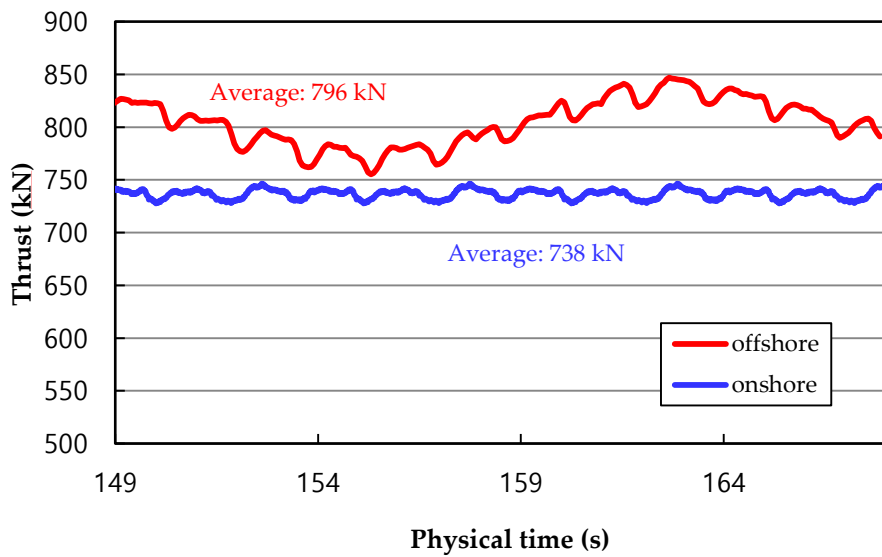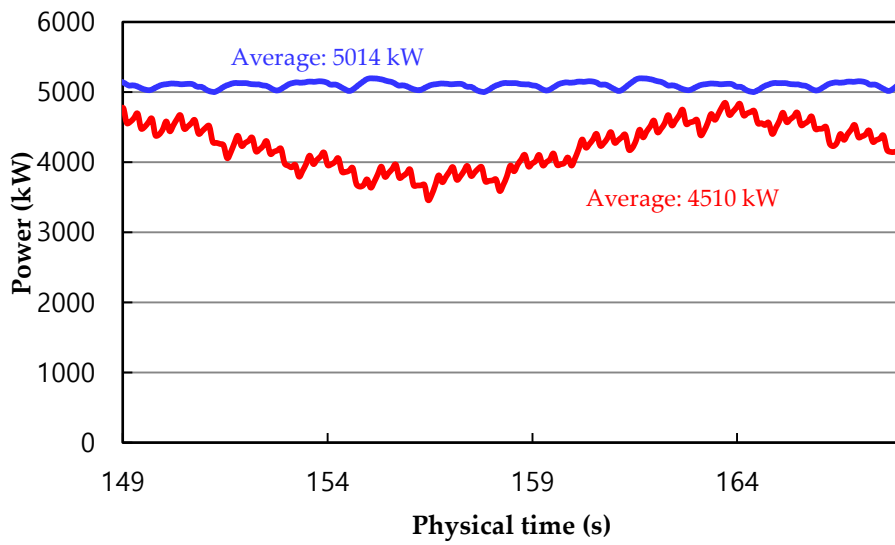
- 53 -

Fig 6-8. Comparison between onshore & offshore

Conclusion

This investigation involved a CFD numerical analysis for a semi-submersible type FOWT used in Phase II of the OC5 project, by advanced DFEI method and overlap mesh technology. The full-configuration FOWT in wind-wave excitation condition was successfully preformed, while simultaneous considering wind turbine movement due to 6-DOF platform dynamics. The RAOs of surge, heave, and pitch were compared to the MARIN test data and data in previous studies where only the wave condition was considered. A slight discrepancy was observed between the CFD studies with regard to the pitch, possibly because of the different physical properties of the platform and mooring lines in the OC4 and OC5 projects. There was a relatively large discrepancy in the hydrodynamic response, which can induce large deviations in the prediction procedure. In particular, the natural period of the pitch showed a 21% discrepancy in the OC4 and OC5 projects, as indicated by the results of the free decay test of the pitch and the numerical discrepancy in the RAOs in the regular wave test.

Further, unsteady blade-tip vortices and strong flow interactions with the turbulent wakes of the tower due to the surge motion of the platform were successfully simulated and visualized using the advanced DFBI and VOF methods. The power and thrust force of the FOWT increased when the floating platform moved in the upwind direction, while the aerodynamic loads decreased as the pitch motion reversed its direction. This can be explained by the variation in the angle of attack for each blade section when the FOWT system experiences pitch motions. All the 3-DOFs, including heave, surge and pitch had smaller amplitudes compared to the results in the regular wave test without wind conditions. Incoming wind from the x direction obviously had a significant effect on the restoring force in the mooring line, and as a result, the whole FOWT system cannot be restored back to the equilibrium position as in the regular wave test.

In addition, a relatively heavy load on the hub and blades was observed for the FOWT compared with the onshore wind turbine. This was because of the thrust force acting on the

top of the tower, due to which the platform moves in the upwind direction to offset the capsizing moment induced by the thrust force. With regard to the power curve, a 10% decrease was observed for the floating offshore wind turbine, which is likely due to the smaller project area and relative income wind speed when the platform experiences pitch motion. Overall, there was a greater variation in the power than in the thrust force, that is, the power output was more sensitive than the thrust force to platform motions.

Till date, all the published studies based on the OC4 project, a code-to-code comparison project carried out in 2013, show large discrepancies with respect to the experimental test data of OC5 project. This study could be a good reference for future research, as there has not been any specific CFD research based on OC5 test data until now. Examination of the OC5 Phase II project, with a CFD code, which has a higher-fidelity model of the underlying physics, could help determine if there are some deficiencies in the hydro dynamic models being employed by participants in OC5 code-to-test project [18].

References

1. Jonkman, J.M. Dynamics Modeling and Loads Analysis of an Offshore Floating Wind Turbine, Doctoral Dissertation, University of Colorado, Colorado, 2007.
2. Sebastian, T.; Lackner, M.A. Development of a free vortex wake method code for offshore floating wind turbines. *J. Renew. Energy* **2012**, 46, 269-275.
3. Fernandez-Gamiz, U.; Zulueta, E.; Boyano, A.; Ansoategui, I.; Uriarte, I. Five Megawatt Wind Turbine Power Output Improvements by Passive Flow Control Devices. *J. Energies* **2017**, 10(6), 742
4. Fernandez-Gamiz, U.; Errasti, I.; Gutierrez-Amo, R.; Boyano, A.; Barambones, O. Computational Modelling of Rectangular Sub-Boundary Layer Vortex Generators. *J. Applied Sciences* **2018**, 8(1), 138
5. Nematbakhsh, A.; Bachynski, E.E.; Gao, Z.; Moan, T. Comparison of wave load effects on a TLP wind turbine by using computational fluid dynamics and potential flow theory approaches. *J. Appl. Ocean Res* **2015**, 53, 142-154.
6. De Vaal, J.B.; Hansen, M.O.L.; Moan, T. Effect of wind turbine surge motion on rotor thrust and induced velocity. *J. Wind Energy* **2014**, 17 (1), 105-121
7. Zhao, W.; Wan, D. Numerical study of interactions between phase II of OC4 wind turbine and its semi-submersible floating support system. *J. Ocean Wind Energy* **2015**, 2 (1), 45-53.
8. Tran, T.T.; Kim, D.H.; Song, J. Computational fluid dynamic analysis of a floating offshore wind turbine experiencing platform pitching motion. *J. Energies* **2014**, 7 (8), 5011-5026.
9. Tran, T.T.; Kim, D.H. The coupled dynamic response computation for a semi-submersible platform of floating offshore wind turbine. *J. Wind Eng. Industrial Aerodynamics* **2015**, 147,104-119.
10. Liu, Y.; Xiao, Q.; Incecik, A.; Wan, D.C. Investigation of the effects of platform motion on the aerodynamics of a floating offshore wind turbine. *J. Hydrodynamics, Ser. B* **2016**, 28 (1), 95-101.
11. Ren, N.; Li, Y.; Ou, J. Coupled wind-wave time domain analysis of floating offshore wind turbine based on Computational Fluid Dynamics method. *J. Renew. Sustain. Energy* **2014**, 6 (2), 1-13.
12. Quallen, S.; Xing, T.; Carrica, P.; Li, Y.; Xu, J. CFD simulation of a floating offshore wind turbine system using a quasi-static crowfoot mooring-line model. *J. Ocean Wind Energy* **2014**, 1 (3), 143-152.
13. Tran, T.T.; Kim, D.H. Fully coupled aero-hydrodynamic analysis of a semisubmersible FOWT using a dynamic fluid body interaction approach. *J. Renew. Energy* **2016**, 92, 244-261.
14. Gueydon, S. Aerodynamic damping on a semisubmersible floating foundation for wind turbines. *J. Energy Procedia* **2016**, 94, 367-378.
15. Chen, J.; Hu, Z.; Wan, D.; Xiao, Q. Comparisons of the dynamical charateristics of a semi-submersible floating offshore wind turbine based on two different blade concepts.

J. Ocean Engineering **2018**, 153, 305-318.

16. Dunbar, A.J.; Craven, B.A.; Paterson, E.G. Development and validation of a tightly coupled CFD/6-DOF solver for simulating floating offshore wind turbine platforms. *J. Ocean Engineering* **2015**, 110, 98-105.

17. Coulling, A.J.; Goupee, A.J.; Robertson, A.N.; Jonkman, J.M.; Dagher, D.J. Validation of a FAST semi-submersible floating wind turbine numerical model with DeepCwind test data. *J. Renew. Sustain. Energy* **2013**, 5, 16-23

18. Robertson, A. OC5 Project Phase II: Validation of Global Loads of the DeepCwind Floating Semisubmersible Wind Turbine. *J. Energy Procedia* **2017**, 137, 38-57

19. Menter, F.R. Two-Equation Eddy-Viscosity Turbulence Models for Engineering Applications. *J. AIAA* **1994**, 32, 1598-1605

20. Tran, T.T.; Kim, D.H. A CFD study into the influence of unsteady aerodynamic interference on wind turbine surge motion. *J. Renewable Energy* **2016**, 90, 204-228

21. Sivalingam, K.; Narasimalu, S. Floating Offshore Wind Turbine Rotor Operating State-Modified Tip Loss Factor in BEM and Comparison with CFD. *J. Technical Research and Applications* **2015**, 3, 179-189

22. Hsu, M.C.; Bazilevs, Y. Fluid-structure interaction modeling of wind turbines: simulating the full machine. Doctoral Dissertation, Iowa State University, Iowa, 2012

23. Siddiqui, M.S.; Rasheed, A.; Kvamsdal, T. Quasi-Static & Dynamic Numerical Modeling of Full Scale NREL 5MW Wind Turbine. *J. Energy Procedia* **2017**, 137 , 460-467

24. Liu, Y.; Xiao, Q.; Incecik, A.; Wan, D. Establishing a fully coupled CFD analysis tool for floating offshore wind turbines. *J. Renewable Energy* **2017**, 112, 280-301

25. Tezdogan, T.; Demirel, Y.K.; Kellett, P.; Khorasanchi, M.; Incecik, A.; Turan, O. Full-scale unsteady RANS CFD simulations of ship behavior and performance in head seas due to slow steaming. *J. Ocean Engineering* **2015**, 97, 186-206